*Sensors and Materials*, Vol. 35, No. 1 (2023) 39–73
MYU Tokyo



S & M 3154

# Gasochromic Hydrogen Sensors: Fundamentals, Recent Advances, and Perspectives

Huan Liu,* Zhe Yang, Lin Wang, Ping Yu,
Zetian Kang, Qian Wu, Chen Kuang, and Anfeng Yu

State Key Laboratory of Safety and Control for Chemicals,
Sinopec Research Institute of Safety Engineering Co., Ltd., Qingdao City 26600, P. R. China

(Received November 11, 2022; accepted January 16, 2023)

***Keywords:*** hydrogen sensor, gasochromic, $WO_3$ nanostructures, flexible fabrication

Hydrogen ($H_2$) is recognized as a vital solution for constructing a sustainable energy society owing to its abundance, high efficiency, and lack of pollution. However, $H_2$ is the lightest gas on earth and can embrittle metals, leading to hydrogen leakage. Because hydrogen has a wide flammability range of 4–74 vol.% in air and low ignition energy, it is crucial to identify hydrogen leakages quickly and efficiently to ensure safety. Although various hydrogen sensors have been developed, gasochromic hydrogen sensors, which are based on color changes caused by gasochromic nanomaterials, show great potential for use in the future hydrogen-based world because they are inexpensive, change color very quickly, and work at room temperature. This technical paper focuses on gasochromic hydrogen sensors. First, gasochromic mechanisms based on $WO_3$ nanomaterials are introduced, and three aspects of state-of-the-art research, $WO_3$ nanomaterials with novel structures, noble metals to promote reactions, and flexible fabrication, are presented. Research on the former two aspects aims to develop high-performance gasochromic nanomaterials, and research on flexible fabrication, i.e., transforming nanomaterials into potential hydrogen sensors, is reviewed here for the first time. In addition, other non-$WO_3$-based gasochromic systems are briefly reviewed. Finally, this technical paper provides a brief perspective for future research.

## 1. Introduction

Hydrogen ($H_2$) is recognized as a vital solution for constructing a sustainable energy society,[1] owing to its advantages of being a clean, sustainable, and abundant fuel with high energy density.[2,3] $H_2$ can be produced by splitting water through a variety of mature technologies that use not only fossil fuels such as coal, petroleum, and methane[4,5] but also renewable energies including wind,[6,7] nuclear power,[8] and so forth.[9,10] Thus, hydrogen is regarded as a promising next-generation energy source. Owing to the substantial progress in fuel cells, hydrogen can be utilized to power vehicles.[11,12] However, $H_2$ is not only flammable in a wide concentration range of 4–74 vol.% in air but also has the lowest ignition energy of 0.017 mJ

*Corresponding author: e-mail: liuhuan_china@163.com
https://doi.org/10.18494/SAM4244

ISSN 0914-4935 
https://myukk.org/

among all gases.[13] Moreover, $H_2$ is colorless, odorless, and tasteless,[14] and once a hydrogen leakage occurs, it is very difficult for human beings to detect it.[15] In addition, hydrogen can embrittle materials,[16,17] leading to the failure of materials or components and hydrogen leakage. Therefore, the detection of hydrogen leakage is crucial to ensure safety.

Several categories of nanomaterials can react with $H_2$ and produce sensing signals, such as electrochemical,[18] chemoresistive,[19,20] optical,[21,22] mechanical,[23] and other signals,[24,25] which can be used to develop hydrogen sensors. Therefore, there have been numerous studies on hydrogen sensors. Several reviews focusing on hydrogen sensors have also been published. Ai *et al.* reviewed hydrogen sensors based on plasmonic mechanism.[26] Wang *et al.* reviewed fiber optical hydrogen sensors.[27] Chen *et al.* reviewed optical hydrogen sensors derived from metal hydrides.[28] Lee *et al.* reviewed hydrogen sensors using Pd nanogaps on an elastomeric substrate,[29] and Ajayan *et al.* reviewed hydrogen sensors based on AlGaN/GaN-heterostructure Schottky diode/HEMT structures.[30]

The United States Department of Energy (DOE) set some performance targets for hydrogen sensors for stationary and automotive applications.[2,31] For example, in terms of stationary applications, the dynamic range and detection limit of an ideal hydrogen sensor are both less than 4 vol.%, and the response and recovery times are both no more than 30 s. Moreover, an acceptable price of a hydrogen sensor (no more than $40 per unit) is also suggested. When it comes to mobile applications, the detection limit is less than 0.1 vol.%, and the response/recovery times are reduced to no more than 1/1 s, respectively. Current hydrogen sensors are mainly based on chemoresistive or electrochemical mechanisms. These devices are relatively large and expensive. Furthermore, high operation temperatures are often required,[32] leading to increased danger of explosion when coupling with the low ignition energy of hydrogen.

Gasochromic hydrogen sensors, which rely on changes in the optical properties of gasochromic materials after exposure to a $H_2$ gas environment, have several advantages making it possible for them to meet the targets set by DOE.[33] First, gasochromic hydrogen sensors work at room temperature and do not require an external electrical input,[34] reducing the risks of hydrogen explosion.[35,36] Second, a color change occurs when they are exposed to hydrogen, making a hydrogen leakage visible to the naked human eye. Third, gasochromic hydrogen sensors are usually inexpensive and can meet the price target of DOE.[37] Therefore, research into gasochromic hydrogen sensing has attracted ever-increasing attention.

Among the gasochromic materials, tungsten trioxides ($WO_3$) have been extensively investigated for the following reasons. First, $WO_3$ is a multi-phase metal oxide, including monoclinic, cubic, tetragonal, orthorhombic, and triclinic phases,[38,39] and a meta-phase, hexagonal $WO_3$, has also been reported.[40,41] Second, the morphology of $WO_3$ can be adjusted by either chemical or physical methods.[42,43] Typical morphologies of $WO_3$ nanoparticles are nanoplates,[44,45] nanofibers,[46,47] nanospheres,[48] nanorods,[49,50] and hierarchical structures.[51,52] Third, $WO_3$ has been investigated as efficient functional nanomaterials for sensing various gases, such as $H_2$,[53,54] acetone,[55,56] $H_2S$,[57,58] $NO_2$,[59,60] and $NH_3$.[61] Therefore, in this review paper, we mainly focus on the gasochromic mechanisms and reactions originating from $WO_3$ nanomaterials. First, the gasochromic mechanisms of hydrogen sensing, mainly based on $WO_3$ nanomaterials, are introduced, aiming to provide an understanding of the

gasochromic reactions. Then state-of-the-art advances in gasochromic hydrogen sensors are reviewed from three aspects; $WO_3$ nanomaterials with novel structures, noble metals with promoting effect, and the flexible fabrication of gasochromic devices. Research on the former two aspects aims to develop high-performance gasochromic nanomaterials, while flexible fabrication, in which nanomaterials are transformed to potential hydrogen sensors, is reviewed for the first time. Other gasochromic sensors are also briefly discussed. Finally, a perspective on gasochromic hydrogen sensing research is given.

## 2. Gasochromic Mechanisms

Gasochromic materials change their optical properties, such as reflectivity and transmittance, when exposed to gases.[62] $WO_3$,[34,63] $MoO_3$,[64,65] and vanadium oxides[66,67] are the main gasochromic materials, among which $WO_3$ has attracted the most attention. Because $WO_3$ is the most extensively investigated nanomaterial for gasochromic reactions, several models have been proposed to reveal its gasochromic mechanisms. Among them, the oxygen vacancy model proposed by Geory *et al.*[68,69] and the double-injection model by Lee *et al.*[70] have been widely accepted.

By investigating gasochromic films of $WO_3$ decorated by platinum, Geory *et al.* proposed that adsorbed $H_2$ dissociates on a Pt layer and is transferred to the $WO_3$ surface, forming W–OH groups. Diffusion process models predict that two protons, instead of a single proton, interact with W centers to form $H_2O$. As water is formed, oxygen vacancies are generated. The coloration proceeds by the diffusion of these oxygen vacancies from the surface to the interior of the film.[68,69] A stable molecular species forms, which consists of newly formed W–O and broken W–O–W bonds, as revealed by IR spectroscopy. The inserted protons attach to the W–O–W skeleton, forming $W–OH_2$ groups.

Lee *et al.* investigated the gasochromic mechanism of amorphous $WO_3$ film by Raman scattering and isotopic heavy oxygen ($^{18}O$) tests.[70] For the prepared $WO_3$ films, only Raman peaks attributed to $O–W^{6+}–O$ and $W^{6+}=O$ were observed, and after coloration, extra Raman peaks due to $O–W^{5+}–O$ and $W^{5+}=O$ were detected. Isotopic oxygen ($^{18}O$) experiments were performed in which the colored $WO_3$ films were bleached, and the Raman spectra were very similar to those of $WO_3$ films bleached in air. These results support the double-injection model, which has been broadly accepted in the electrochromic field.

The importance of water in the gasochromic effect was revealed by Xu's group.[71] They investigated the coloring/bleaching reactions of $WO_3$ nanowires decorated by Pt and found the existence of localized water molecules in colored $WO_3$ nanowires. The surface reactions can be described in Fig. 1. There existed absorbed oxygen species on the surface of Pt-decorated $WO_3$ nanowires (I), and hydrogen species are dissociated by Pt (II). Subsequently, the hydrogen species react with the absorbed oxygen species to form water molecules, which desorb from the surface. Hydrogen species may also react with the oxygen atoms of $WO_3$ to form localized water molecules (III), and this water may be removed by high-temperature heating.

Chen *et al.* synthesized a $WO_3$ nanowire film by thermal evaporation and thoroughly investigated the gasochromic mechanism by a combination of advanced techniques, including

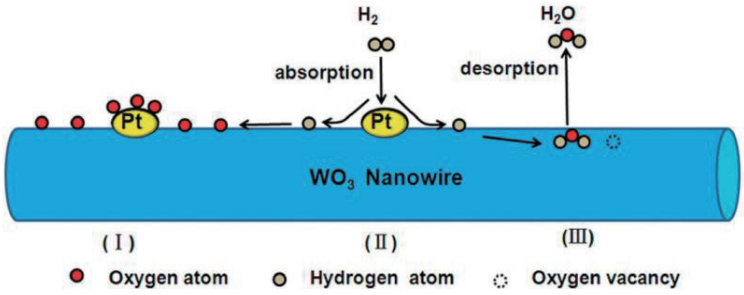


Fig. 1. (Color online) Illustration of gasochromic reaction on Pt-decorated $WO_3$ nanowire. (Reprinted with permission from Ref. 71).

UV–visible–near IR spectroscopy (UV–vis–NIR), X-ray diffraction (XRD), micro-Raman spectroscopy, and X-ray photoelectron spectroscopy (XPS).[72] The XRD results revealed that the phase of as-prepared $WO_3$ nanowires is monoclinic, and the phase of tetragonal hydrogen bronze $H_{0.23}WO_3$ in the colored state was confirmed. This implied that the coloration of the $WO_3$ nanowire was due to the injection of hydrogen. Moreover, $H_{0.23}WO_3$ was unstable in an oxidizing atmosphere, and the bleaching process was investigated by *in situ* XRD. The injected hydrogen can also reduce tungsten from 6+ to 5+, as revealed by XPS. The changes in the $WO_3$ phases and the valence of tungsten ions contribute to the coloration process.

Similar results were also reported by Inouye *et al.* Using elastic recoil detection analysis (ERDA) and Rutherford backscattering spectroscopy, they found that the compositions and crystalline structures of $WO_3$ differed before and after gasochromic reactions.[73] The hydrogen concentration in the oriented $WO_3$ films was 0.24 H/W, which increased to 0.47 H/W after coloration, while the crystalline structure changed from monoclinic to tetragonal. The results imply that the gasochromic coloration involved the incorporation of H atoms into the crystalline lattice, which was attributed to the formation of hydrogen tungsten bronze ($H_xWO_3$).

Chan *et al.* investigated the hydrogen insertion coefficients in gasochromic tungsten bronze ($H_xWO_3$) based on chemical reaction equilibrium.[74] The nanostructured $WO_3$ films were obtained by sol–gel spin coating, than a Pt layer was sputtered onto the surface. The maximum value of the hydrogen insertion coefficient (x) in the equilibrium tungsten bronze ($H_xWO_3$) in the study was about 0.29, which was slightly higher than the value reported by Inouye *et al.*[73]

Advanced *in situ* analytical technology can capture the dynamic transformation of $WO_3$ nanomaterials, thus contributing to revealing the gasochromic mechanism. Castillero *et al.* elucidated the gasochromic behavior through *in situ* near-ambient photoemission (NAPP) on a $Pt/WO_3$ film.[75] The coloration was attributed to the formation of $W^{5+}$ species, mainly in inner layers of $WO_3$. The NAPP results revealed that hydroxyl groups/water formed and remained at the surface. A possible reaction model has been proposed (Fig. 2), which includes the dissociation of $H_2$ and the spillover of hydrogen atoms from the metal phase to the substrate. When hydrogen is introduced to the reaction system, hydrogen species are formed and spill over the $WO_3$ surface. The hydrogen species then react with oxide anions or hydroxyl groups at the surface to form surface hydroxyl groups or water molecules, respectively. At the same time, the released electrons react with $W^{6+}$ cations in inner layers to form buried $W^{5+}$ species.

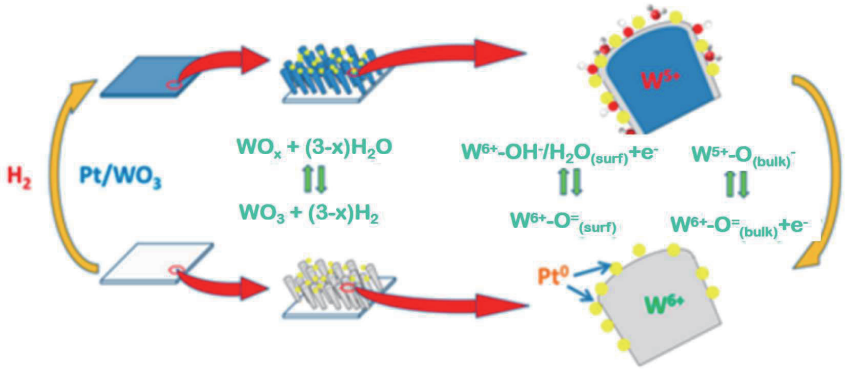


Fig. 2. (Color online) Illustration of gasochromic reaction on Pt/$WO_3$. (Reprinted with permission from Ref. 75).

Nagata *et al.* prepared $WO_3$ thin films by magnetron sputtering on $SiO_2$ glass substrates with substrate temperatures ranging from 300 to 970 K.[76] Then hydrogen incorporation into $WO_3$ films was investigated by ERDA. The average hydrogen concentration, namely, the x-value of the $H_xWO_3$ film, increased with increasing substrate temperature during sputtering. The effective incorporation of hydrogen and the enhanced gasochromic performance were due to the high diffusivity of hydrogen in the oriented crystalline structure of $WO_3$.

Gao *et al.* revealed the mechanism of the gasochromic responses of $WO_3$ thin films activated by UV irradiation,[77] and found that the porosity of $WO_3$ films markedly increased upon UV irradiation, which led to the formation of $H_xWO_3$ ($x$ = 0.17). Previous research studies revealed that further increasing the hydrogen content of $H_xWO_3$ ($x$ = 0.32) led to the transition from insulating to metallic,[78] and that after hydrogen incorporation, blue-colored tungsten oxides were formed.[79] Gasochromic results revealed that UV irradiation is useful for fast coloration. They proposed a new model based on a resistor and capacitor circuit and double-injection theory. The injection current depended on the ion ($R_i$) and electron ($R_e$) resistance values in the circuit, especially the larger values. When the $WO_3$ films were irradiated by UV, the newly formed $H_xWO_3$ phase led to low resistance. Therefore, the low $R_i$ from $WO_3$ and the low $R_e$ from $H_xWO_3$ both contributed to enhanced gasochromic performance.

In addition to the experimental investigations, theoretical research has also provided an in-depth understanding of the gasochromic mechanisms. Xi *et al.* investigated hydrogen spillover onto a $WO_3$ (0 0 1) surface promoted by a platinum catalyst then into the bulk through density functional theory (DFT) calculations.[78] The results demonstrated that water played a vital role in facilitating the hydrogen spillover process and H incorporation into $WO_3$, and diffusion throughout the lattice was attributed to the favorable H-bonding interactions available during the entire process.

Cheng *et al.* explored the microscopic nature of CO, $H_2$, $NH_3$, and $NO_2$ on the surface of $WO_3$ (0 0 1) through DFT calculations and experimental research.[80] The results showed that after gas adsorption, the $WO_3$ surface undergoes reconstruction, leading to the localization of surface electrons and changes in the electric (sensing) signals. Experimental results on absorption at 100 °C under an argon atmosphere showed that hydrogen exhibited a faster recovery time but a lower sensitivity and shorter response time than other gases.

Although the gasochromic phenomenon of hydrogen sensing was reported by Deb about half a century ago,[81] the fundamental understanding of the gasochromic effects of $WO_3$ nanomaterials still requires further research, especially on the physicochemical and electronic changes occurring to $WO_3$ nanomaterials in gasochromic reactions. To reveal the reaction mechanisms, a possible route may involve the combination of well-defined $WO_3$ nanomaterials with a specific structure and *in situ* analytical techniques, such as XRD, XPS, ERDA, and NAPP. DFT calculations are also expected to make a major contribution to understanding the changes of $WO_3$ in gasochromic reactions.

## 3. State-of-the-art Research

Advanced gasochromic hydrogen sensors have been increasingly required with the rapid development of a hydrogen-based society. The exploration of $WO_3$ with novel structures, research into the noble metals to promote reactions, and the flexible fabrication of gasochromic materials are the main aspects of research. The following subsections discuss technical papers on the state-of-the-art research from these three aspects.

### 3.1 $WO_3$ nanomaterials with novel structures

$WO_3$ materials with novel structures, such as specific phases, uniform morphologies, porous channels, and so forth, play a vital role in developing high-performance gasochromic hydrogen sensors. Therefore, both physical and chemical methods have been employed to synthesize $WO_3$ materials, and gasochromic performances towards hydrogen have been systematically investigated to provide ideal nanomaterials for further applications.

Organic templates have often been used in the preparation of nanoporous $WO_3$ materials, although high-temperature annealing to remove them can lead to structure collapses, destroying the nanoporous structure. Xue *et al.* have recently adopted a novel strategy to synthesize nanoporous $WO_3$ films with the assistance of UV irradiation,[43] the scheme of which is shown in Fig. 3. An organic template of poly(ethylene glycol)-block-poly(propylene-glycol)-block-poly (ethylene glycol) (P123) was used to synthesize nanoporous $WO_3$ films, which was removed under UV radiation in a low-temperature environment while maintaining the nanoporous structure. Figures 3(b)–3(e) show SEM and TEM images of $WO_3$ films, which exhibited a pore size distribution from 10 to 16 nm. With the help of UV radiation, high-temperature annealing was avoided, leading to the formation of nanoporous $WO_3$ films. A $SiO_2$-$PdCl_2$ film was deposited as a catalyst layer onto the nanoporous $WO_3$ films in accordance with the work of Wang *et al.*,[82] and gasochromic performances are shown in Figs. 3(f) and 3(g). The nanoporous $WO_3$ films showed rapid coloring in 10% $H_2$, with a 90% transmittance change in 20 s, while the reverse change occurred in 10 s for bleaching in pure $O_2$. A nanoporous $WO_3$ film annealed at 200 °C was prepared for comparison, and the coloring/bleaching times were 40 s/20 s, respectively, with the long times mainly attributed to pore collapse.

Kalanur *et al.* investigated novel $WO_3$ materials with ultrathin 2D morphologies and their gasochromic performances.[83] Owing to their enhanced surface/volume ratios, ultrathin 2D

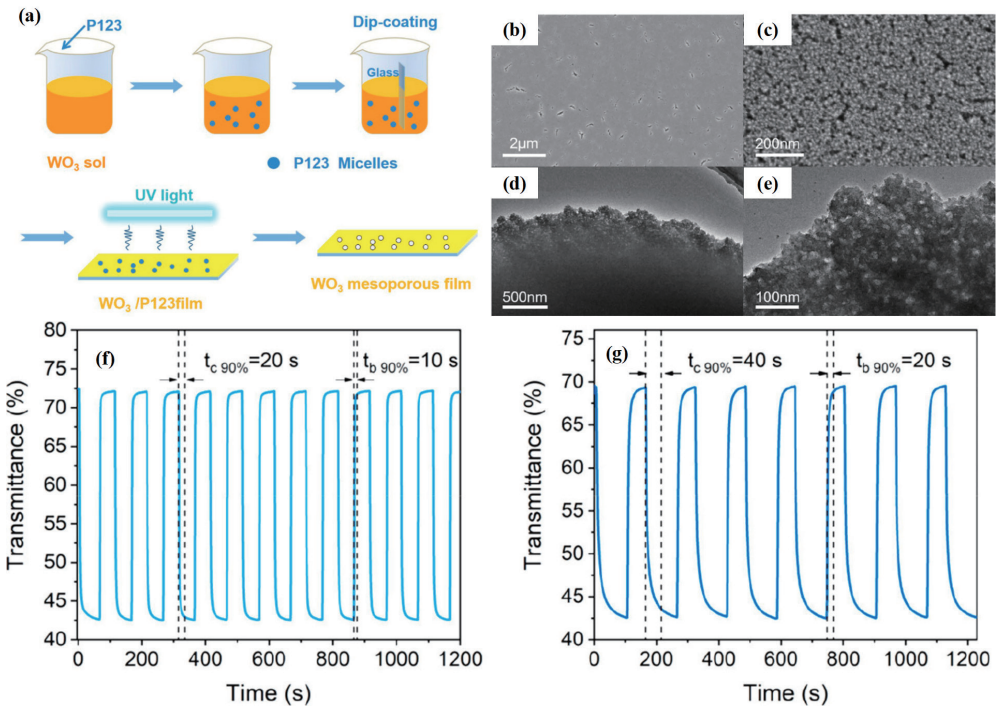


Fig. 3. (Color online) (a) Scheme of preparing nanoporous $WO_3$ films; SEM (b) and (c) and TEM (d) and (e) images with different magnifications of $WO_3$ films; and gasochromic cycles of $WO_3$ film (f) and $WO_3$ film annealed at 200 °C (g). (Reprinted with permission from Ref. 43).

nanomaterials have efficient physisorption and chemisorption properties, making them suitable for sensing. Kalanur *et al.* synthesized ultrathin 2D $WO_3$ nanoplates through the sol–gel method (Fig. 4) and introduced Pd nanoparticles to decorate $WO_3$ nanoplates by photochemical deposition.[84] The 2D Pd-$WO_3$ materials were fabricated on filter paper, and their gasochromic performances towards hydrogen are shown in Fig. 4(e). Eye-readable color changes from light green-gray to dark blue were detected. When the concentrations of $H_2$ were 20, 10, and 4%, the coloration times were about 4, 6, and 30 s, respectively. However, for lower concentrations of $H_2$ (1 and 0.1%), partial coloration was detected even after long exposure times. Compared with the aforementioned Pd-$WO_3$ matrix, the ultrathin 2D Pd-$WO_3$ materials were about 10 times faster, which is attributed to the rapid diffusion of hydrogen atoms throughout the novel $WO_3$ structure. A mechanism describing the gasochromic reaction was proposed, as shown in Fig. 4(f), which includes the absorption of hydrogen into H atoms and its dissociation, transformation onto the surface of $WO_3$ through spillover, and reaction with oxygen ions of $WO_3$ to form localized water molecules with the creation of oxygen vacancies.

Lee *et al.* employed a novel electrostatic spray deposition (ESD) method to fabricate a simple, facile, and cost-effective $WO_3$-based sensor.[42] Compared with common fabrication strategies, such as vacuum-based or wet-chemical-based processes, ESD technology results in the deposition of a more uniform structure with more controllable porosity and an increased reaction area. Moreover, the atmospheric-based ESD process is cost-effective and highly reproducible.

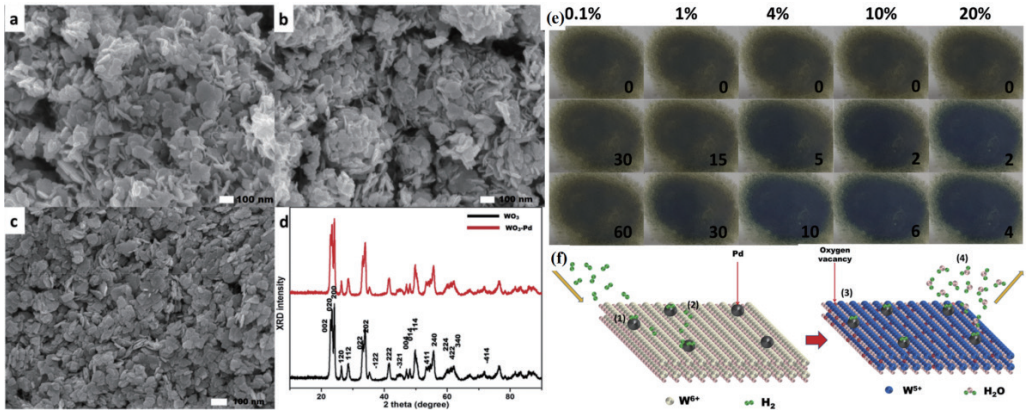


Fig. 4. (Color online) SEM images of (a) $WO_3$, (b) Pd-$WO_3$, and (c) Pd-$WO_3$ on filter paper sensor. (d) XRD patterns of $WO_3$ and $WO_3$-Pd. (e) Photographic images of gasochromic reactions and (f) mechanism of gas-sensing steps. (Reprinted with permission from Ref. 84).

Figure 5(a) shows a schematic of the ESD process for preparing a Pd-$WO_3$ gasochromic sensor. By adjusting the Pd/$WO_3$ molar ratio and layer thickness, six Pd-$WO_3$ materials with respect to $WO_3$:Pd were fabricated, which were 25:1, 50:1, 75:1, 100:1, 125:1 to 150:1, respectively, with a thickness of 5 mm. The hydrogen sensors exhibited excellent performances towards 1 vol.% $H_2$ at room temperature. Figure 5(b) shows optical images of the Pd-$WO_3$ sensors before and after exposure to 1% hydrogen gas. An optimized hydrogen sensor with a $WO_3$:Pd molar ratio of 125:1 was obtained, and a color change was clearly observed by the naked eye within 15 s. Figure 5(c) shows photographs of the optimized hydrogen sensor attached to a possible hydrogen leakage (1 mm hole) site in a hydrogen pipeline, and a color change was observed in 15 s.

Foroushani *et al.* obtained tungsten oxide nanofibers with average diameters of 103, 181, and 293 nm by electrospinning.[47] Proxopolytungstic acid (PPTA) was used as the tungsten precursor, and polyvinylpyrrolidone (PVP) was added to form a homogenous solution. Then $WO_3$ nanofibers with the average diameters of 103, 181, and 293 nm were produced (Fig. 6), and $PdCl_2$ was added to activate the nanofibers. The gasochromic performances towards 10% $H_2$/Ar were tested, and the results are shown in Fig. 6(g). The colors of the three $WO_3$ nanofibers changed from pale yellow to blue within 2 min. XRD results revealed that the phases of the as-prepared $WO_3$ nanofibers were monoclinic, and that after exposure to hydrogen, a new phase attributed to hydrogen tungsten oxide ($H_{0.23}WO_3$) was detected, which is similar to the results reported by Chen *et al.*[72] When the colored $WO_3$ nanofibers were placed in air, the pale yellow color returned, and the original monoclinic microstructure was recovered.

Hsu *et al.* prepared $WO_3$ thin films on microscope slide glass substrates by pulsed laser deposition (PLD), and Pt was sputtered on the $WO_3$ surface as a catalyst layer.[85] When the substrates were pretreated at room temperature and 250 °C, the obtained $WO_3$ films had an amorphous structure, while the $WO_3$ film became a highly crystalline monoclinic structure at a substrate temperature of 500 °C. However, for the $WO_3$ film prepared at 500 °C, poor gasochromic performance was observed even after prolonged hydrogen exposure (2 min). The

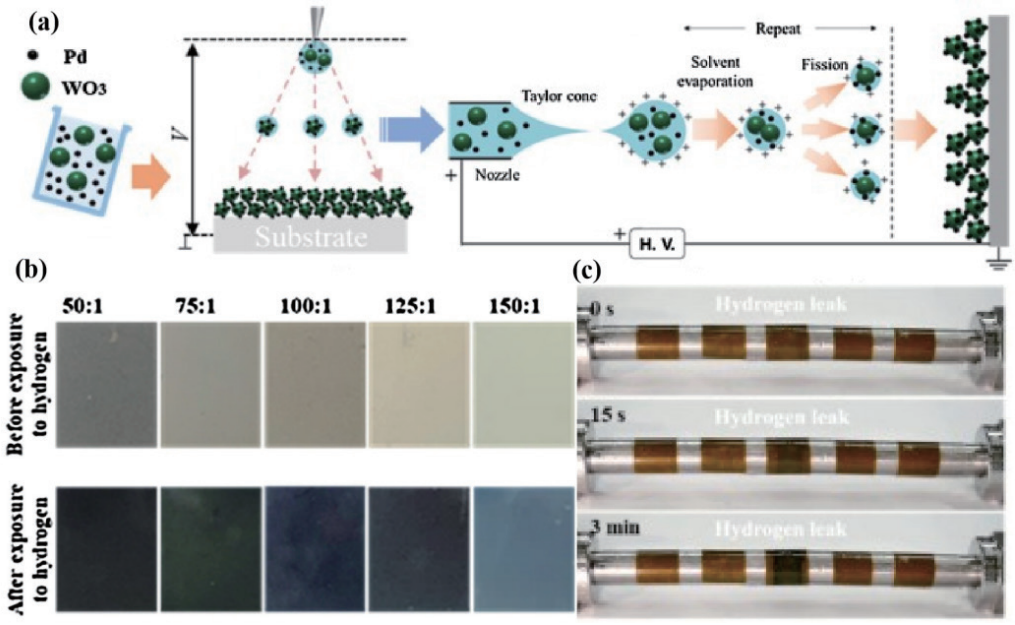


Fig. 5. (Color online) (a) Schematic of ESD process for fabricating $WO_3$-Pd sensor. (b) Optical images of all sensors before and after exposure to 1% hydrogen gas. (c) Photographs of tape-type sensors attached to a gas pipeline at 0 s, 15 s, and 3 min. (Reprinted with permission from Ref. 42).

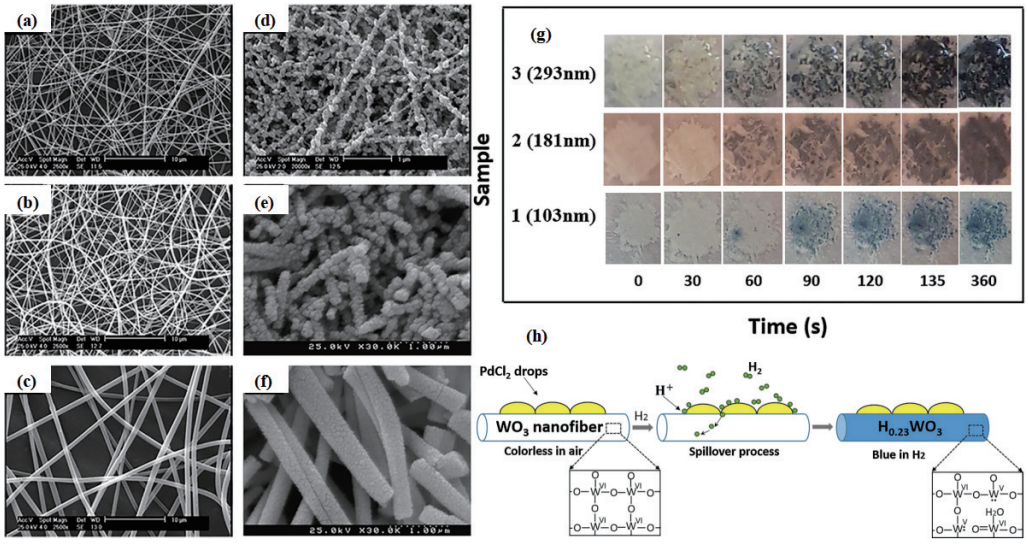


Fig. 6. (Color online) SEM images of PPTA–PVP nanofibers [(a), (b), and (c) before calcination] and tungsten oxide nanofibers [(d), (e), and (f) after calcination]. (g) Color changes of nanofibrous $WO_3$ in 10% $H_2$/Ar gas. (h) Schematic representation of the gasochromic mechanism. (Reprinted with permission from Ref. 47).

$WO_3$ film synthesized at room temperature exhibited large transmittance changes of 59% (at 700 nm) and 34% (at 550 nm) towards 0.5% $H_2$. The response time for coloring/bleaching of the $WO_3$ thin films was less than 1 s with a hydrogen concentration exceeding 1%.

The effects of the O/W ratio and structure on gasochromic films were systemically investigated by Yamamoto *et al.*[86] It was found that $WO_3$ with an amorphous structure and an O/W ratio of 3:1 exhibited superior gasochromic performance, while non-stoichiometric or crystalline $WO_3$ led to a poor activity.

Li *et al.* reported the gasochromic performance and durability of $WO_3$-based films prepared by dip-coating.[87] The $WO_3$ films were enhanced by the introduction of $SiO_2$ particles, forming a $WO_3$-$SiO_2$ nanoporous supporting network, and Pd was dispersed as a catalyst. The $WO_3$-$SiO_2$ films exhibited ultrafast coloring/bleaching rates, with a coloring rate of 14.8%/s and a bleaching rate of 44.1%/s in pure oxygen (1.95%/s in air). As a comparison, the coloring and bleaching rates of pure $WO_3$ films promoted by Pt were 2.84 and 7.18%/s in pure $O_2$ (0.19%/s in air), respectively. The excellent coloring/bleaching performance of the $WO_3$-$SiO_2$ films was ascribed to the amorphous structure, which provides a large surface area and many diffusion channels. A novel cross-linked microstructure was formed in the $WO_3$-$SiO_2$ matrix, and the distribution of Pd nanoparticles in the film enhanced the catalytic activity, which also contributed to the enhanced gasochromic performances.

Wang *et al.* prepared two $WO_3$-based gasochromic films by combining the sol–gel route and dip-coating,[82] and the structures of two films are shown in Figs. 7(a) and 7(b). One film was composed of a $WO_3$ layer with $PdCl_2$ as a catalyst, and in the other film, a $WO_3$ layer was covered by a $SiO_2$ layer, while the $PdCl_2$ catalyst was only in the $SiO_2$ layer. The $WO_3$/$SiO_2$+Pd film exhibited a longer gasochromic cycle lifetime and a shorter response time than the $WO_3$+Pd film towards diluted hydrogen. A scheme of the splitting and diffusion of hydrogen is depicted in Fig. 7(c). The edge-sharing W–O–W structure improves the cycle lifetime, and the pre-splitting hydrogen atoms in the $SiO_2$-Pd layer diffuse faster than hydrogen molecules, resulting in a faster gasochromic process.

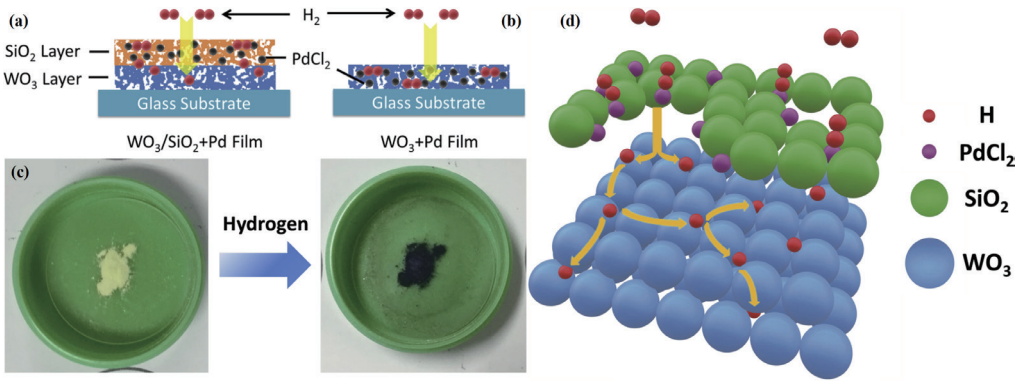


Fig. 7. (Color online) (a) Design of the $WO_3$/$SiO_2$+Pd film and (b) $WO_3$+Pd film. (c) Gasochromic performances of nano-$WO_3$. (d) Scheme of splitting and diffusion of hydrogen in $WO_3$/$SiO_2$+Pd film. (Reprinted with permission from Ref. 82).

Chen *et al.* reported a novel optoelectronic Pd-$WO_3$/graphene/Si tandem structure for hydrogen sensing,[88] as shown in Fig. 8. This optoelectronic device mainly includes three layers: Pd-$WO_3$ (400 nm), graphene, and Si. The graphene/Si serves as photodetector layers owing to their photovoltaic property, while the Pd-$WO_3$ film senses hydrogen gas on the basis of its gasochromic character. Upon exposure to hydrogen, the color of the Pd-$WO_3$ film changes to dark blue, and the gasochromic change is synchronously sensed by the graphene/Si photodetector. The optoelectronic gas sensor with this design detected a low concentration of $H_2$ (0.05%). The response time was less than 13 s and the recovery time was 43 s.

Takahashi *et al.* thoroughly investigated the effects of fabrication parameters, i.e., the annealing process, precursor concentration, and catalyst loading, on gasochromic performances towards hydrogen.[89] An annealing temperature of 500 °C was found to be preferable for attaining high sensitivity and a fast response. To obtain a stable gasochromic performance, the minimum annealing time was 0.5 h. Increased Pt loading led to better sensitivity and a faster response, and the optimized molar ratio of Pt to W to maximize sensitivity was 0.35.

Pd/$WO_3$ nanorods prepared through magnetron sputtering with glancing-angle deposition for gasochromic hydrogen detection have been reported.[90] The $WO_3$ nanorods had an average length of 400 nm, a diameter of 50 nm, and a rod separation of 20 nm. Pd/$WO_3$ films were obtained by depositing the nanorods on quartz substrates. The absorbance of the Pd/$WO_3$ film in the 650–1000 nm wavelength range increased by about 51% upon exposure to 0.1% $H_2$ in air.

$WO_3$/glass thin films fabricated by PLD were reported by Behbahani *et al.*, who investigated the effects of substrate temperatures of 25, 100, 200, 300, and 400 °C.[91] $PdCl_2$ solution was introduced as a catalyst, and coloring from the edge to the center was observed in the presence of hydrogen. The $WO_3$/glass films prepared up to 300 °C exhibited amorphous phases, while an orthorhombic structure of $WO_3$ was confirmed at 400 °C. After hydrogen exposure, eye-readable color changes were observed on all the samples, and the color changed from the boundary edge of the catalyst drop, then gradually extended into the center. After hydrogen exposure, $PdCl_2$(aq)/$WO_3$ was reduced to Pd/$WO_3$. The $WO_3$ prepared at 200 °C had the highest gasochromic reaction rate, which was attributed to its high surface porosity.

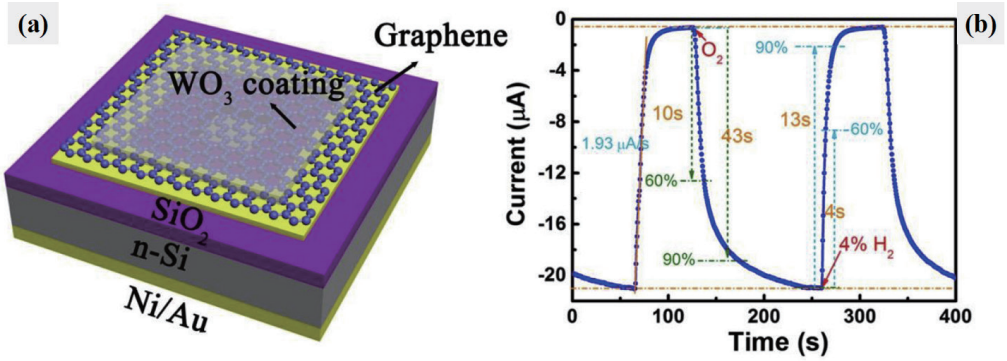


Fig. 8. (Color online) (a) Tilted schematic of device structure and (b) response of the device to 4 vol% $H_2$/Ar. (Reprinted with permission from Ref. 88).

A structure-directing agent has a marked effect on the design of novel $WO_3$ nanomaterials, which can lead to unique and uniform morphologies and highly ordered channels. Feng *et al.* synthesized highly ordered mesoporous $WO_3$ films by a facile template-assisted sol–gel method.[92] A tri-block copolymer, Pluronic F127, with an average molecular weight of 12600 acted as the templating agent, then a rapid thermal process was used to remove the template. Under annealing temperatures of 250 and 350 °C, the highly ordered mesoporous $WO_3$ exhibited an amorphous character, and a monoclinic phase was observed after annealing at 450 °C (Fig. 9). The highly ordered mesoporous $WO_3$ exhibited an enhanced gasochromic performance toward 4% $H_2$-Ar mixture gas, with the transmittance reduced to 5% within 3 s. The fast coloring/bleaching was attributed to the high surface area and short proton diffusion distance of the highly ordered mesoporous $WO_3$ materials.

Polystyrene (PS) microspheres have also been used to synthesize ordered mesoporous $WO_3$ films by a colloidal template method.[93] The $WO_3$ films had a uniform porous structure with average pore diameters (APDs) of 325, 772, and 1119 nm. Pt nanoparticles were introduced through sputtering. Among the three Pt/$WO_3$ films, the one with the APD of 325 nm exhibited the fastest gasochromic activity, which maintained its activity after 100 gasochromic cycles. Li *et al.* reported the synthesis of monoclinic $WO_3$ nanosphere films via the sol–gel method, where the amphiphilic diblock copolymer polystyrene-b-polyacrylic acid (PS-b-PAA) served as a template,[94] and after a Pt layer sputtered, a hydrogen gasochromic device was fabricated. SEM analysis showed that the $WO_3$ nanoparticles had diameters of 200–400 nm, while TEM results revealed that the $WO_3$ nanosphere diameter was 50–500 nm. The color changed from light yellow to blue in about 5–10 s upon exposure to pure hydrogen, and the bleaching time was about 10–20 s.

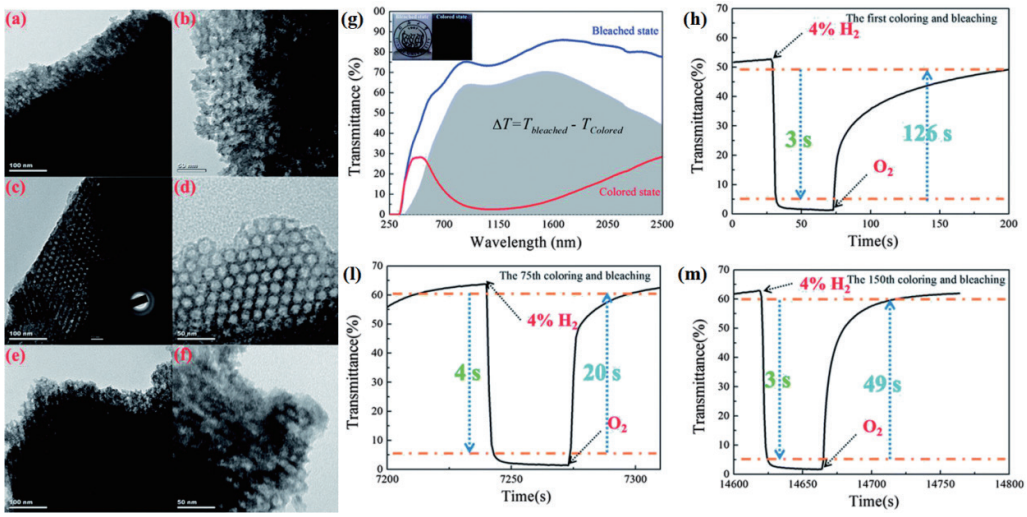


Fig. 9. (Color online) TEM images of $WO_3$ films with various annealing temperatures: (a) and (b) 250; (c) and (d) 350; (e) and (f) 450 °C. (g) Optical modulation ability and (h)–(m) typical coloring/bleaching response of the mesoporous $WO_3$ film. (Reprinted with permission from Ref. 92).

Zhou *et al.* prepared porous $WO_3$ nanosphere films by a template-assisted sol–gel method[95] with Pluronic F127 serving as the template. To remove the template, high-temperature annealing has often been used, which leads to the collapse of the nanostructure. Therefore, as another route to remove F127, solvent extraction followed by annealing at 350 °C was proposed, and the results are shown in Figs. 10(a) and 10(b). A uniform nanosphere film was observed, and no other impurities were detected. The gasochromic results of the $WO_3$ nanosphere films towards 4% $H_2$ with the transmittance recorded at 1000 nm are shown in Figs. 10(c) and 10(d). The coloring/bleaching times of the porous $WO_3$ nanospheres films were 78 and 56 s, respectively, and no obvious loss in gasochromic performance was detected after 50 cycles.

On the basis of photonic crystals, Amrehn *et al.* proposed a rational design of $WO_3$ nanoparticles to reveal in detail the relationship between the chemical reactions and the optical responses toward various concentrations of hydrogen at different temperatures, thus advancing the understanding of the sensing mechanism.[96] Poly(methyl methacrylate) (PMMA) particles were first synthesized, then artificial opals of a PMMA structure matrix were prepared on a glass substrate by drop deposition. Then the artificial PMMA opals were infiltrated with a tungsten-containing solution and heated at 400 °C for 5 h. Finally, the Pt catalyst was introduced through wet impregnation. The $WO_3$ opals showed an immediate response towards $H_2$ concentrations from 0.3 to 10% at temperatures ranging from 100 to 200 °C. For 5% $H_2$ at 200 °C, the response time was less than 1 s.

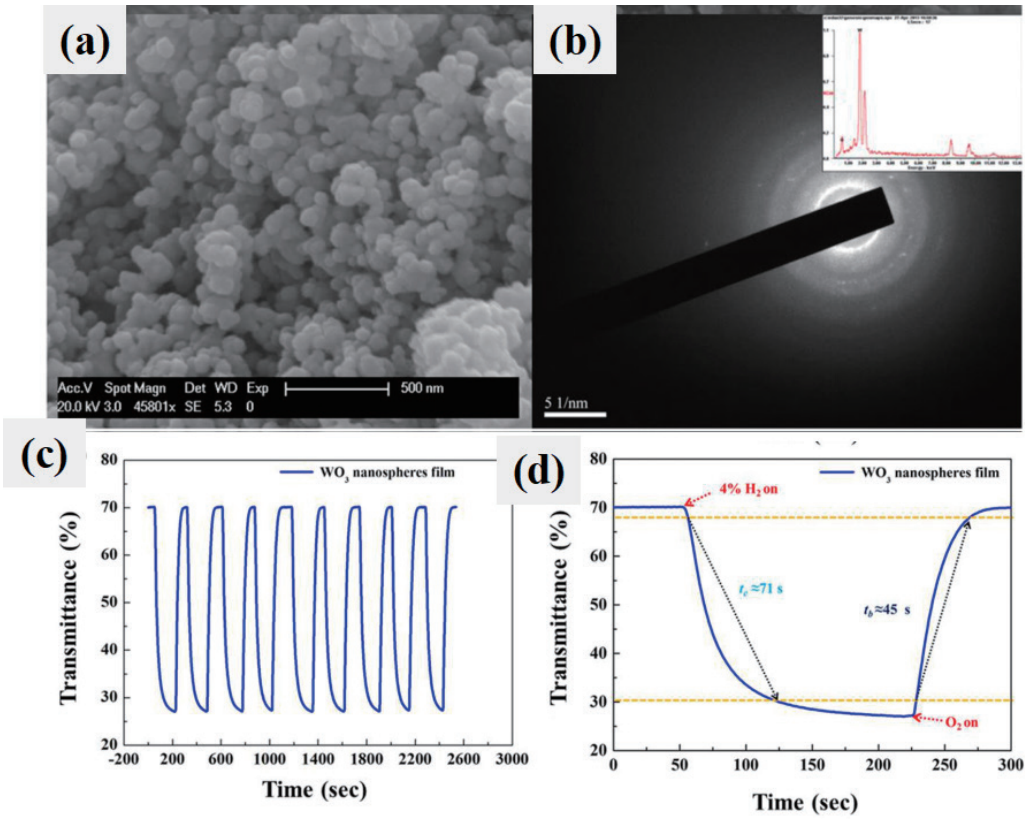


Fig. 10. (Color online) (a) SEM image and (b) SAED pattern of $WO_3$ nanosphere film, and (c) and (d) gasochromic performances of $WO_3$ nanosphere film. (Reprinted with permission from Ref. 95).

### 3.2 Noble metals to promote reactions

Considering that pure $WO_3$ nanomaterials cannot exhibit gasochromic properties at low temperature, noble metals such as Pd, Pt, and Au play vital roles in the gasochromic reaction. They can adsorb, activate and dissociate hydrogen at much lower temperatures than $WO_3$ and even at room temperature. Therefore, the introduction of noble metals and their effects on gasochromic reactions have been investigated in detail.

Garavand *et al.* synthesized $WO_3$ films by PLD and obtained hydrogen sensors after the deposition of Pd nanoparticles.[97] After the PLD of $WO_3$ onto glass substrates, followed by annealing at 250 and 350 ℃ in air, amorphous and crystalline structures were detected, respectively. Then Pd nanoparticles were introduced into $WO_3$ through the hydrogen reduction of drop-drying $PdCl_2$ solution at 60 ℃. Hydrogen sensing experiments at various temperatures showed that the gasochromic performances of the amorphous $WO_3$ decorated by Pd below 100 ℃ remained approximately constant, whereas for the crystalline $WO_3$ sensors, an optimum operating temperature of between 90 and 100 ℃ was found. Moreover, the crystalline $WO_3$ nanoparticles with a low surface-to-volume ratio and negligible diffusion length exhibited less color change above 100 ℃ than the amorphous ones.

Furthermore, the same group investigated the gasochromic performances of $WO_3$ promoted by two noble metal metals, Pt and Pt nanoparticles.[98] The $WO_3$ film was synthesized by PLD and annealed at 250 ℃. The introduction of Pd nanoparticles into the $WO_3$ surface was the same as described before. For the Pt-$WO_3$ samples, the gasochromic performance remained approximately constant above 90 ℃. A higher gasochromic response was observed on the Pt-$WO_3$ samples than on the Pd-activated $WO_3$ samples from 90 to 120 ℃.

The effects of Pt on a $WO_3$ gasochromic film have been investigated by a combination of techniques.[99] Increasing the Pt content on the film led to enhanced changes in transmission, and small and sharp peaks were detected on the $WO_3$ film by atomic force microscopy. However, further increasing the Pt content decreased the transmission, and small and smooth grains were formed. Therefore, considering the balance between the gasochromic performance and the price, an optimal Pt content exists for the gasochromic device. Similar research focusing on the effect of the Pt content was reported by Ranjbar *et al.*[100]

Kalanur *et al.* proposed a green deposition strategy for Pd nanoparticles to promote $WO_3$ nanoparticles, thus obtaining a gasochromic sensor.[84] In the synthesis procedure, electron–hole pairs on $WO_3$ were generated during UV irradiation, and the photogenerated electrons reduced $Pd^{2+}$ to Pd metal nanoparticles [Fig. 11(a)]. Polyvinylpyrrolidone (PVP, MW≈40,000) was introduced to prevent the agglomeration of Pd on the $WO_3$ nanoparticles, leading to well dispersed, uniformly sized, and amount-controlled Pd nanoparticles on $WO_3$. From scanning transmission electron microscopy (STEM) analysis, highly dispersed Pd nanoparticles without apparent aggregation were confirmed [Fig. 11(b)]. The Pd-decorated $WO_3$ nanocomposite was dispersed on filter paper. For 1%, 10%, and pure hydrogen, the coloration times were 240, 75, and 45 s, respectively. When the hydrogen concentration was below 0.1%, no visible color change was obtained. Furthermore, a scheme was proposed to describe the gasochromic reaction, which included $H_2$ adsorption, $H_2$ spillover, H atoms attacking oxygen in the lattice near the surface, the formation of $H_xWO_3$, and the creation of oxygen vacancies by water desorption.

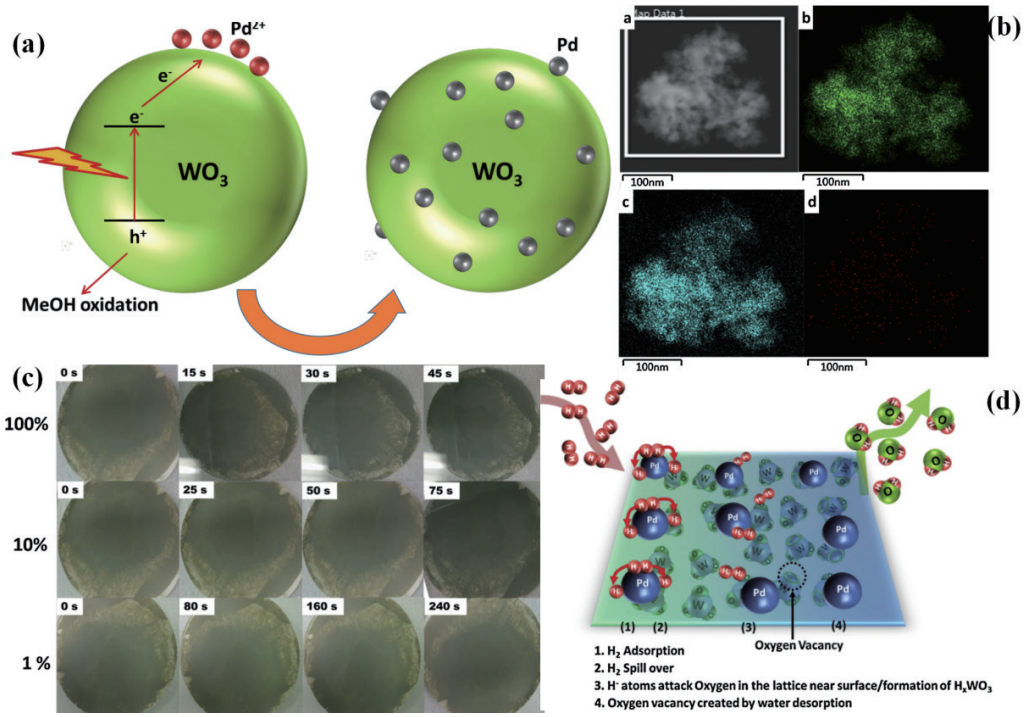


Fig. 11. (Color online) (a) Photochemical deposition of Pd on $WO_3$ nanoparticles. (b) STEM image of Pd-$WO_3$ composite and elemental mapping images. (c) Photographic images of Pd-$WO_3$ nanocomposite on filter paper for different hydrogen concentrations. (d) Mechanism of gasochromic reaction. (Reprinted with permission from Ref. 84).

A similar strategy to reduce a $Pt^{2+}$ precursor to Pt nanoparticles through UV irradiation was reported by Nishizawa *et al.*, thus obtaining a gasochromic film.[101] In this strategy, the photocatalytic property of $WO_3$ was used to reduce Pt, which created a large number of voids in the film. An amorphous $WO_3$ film was spin-coated on a glass substrate, and the Pt precursor was then introduced by the same method. Before drying, the film was irradiated with 365 nm UV light (1 mW $cm^{-2}$) for 15 min under a diluted hydrogen gas (4% in Ar). The obtained Pt-$WO_3$ films showed a fast gasochromic response (5 s) after hydrogen exposure, and the transmittance changed from about 80 to 10% (at a wavelength of 670 nm). Moreover, the switching was maintained after more than 1500 cycles, indicating its durability. The same authors then carried out a comparative study of Pd and Pt nanoparticles dispersed on $WO_3$ films.[102] The noble metals were introduced by a combination of UV irradiation and a $H_2$ gas flow at room temperature. The gasochromic response of the Pd-$WO_3$ film was slower than that of the Pt-catalyzed film, whereas the bleaching speeds were almost the same. The slow coloring of the Pd film was attributed to the inhomogeneity of the Pd nanoparticles.

Okazaki and Johjima investigated the gasochromic responses of Pt/$WO_3$ at various temperatures (from −40 to 100 °C) to evaluate the devices in harsh environments.[62] The sensitivity and response time were strongly dependent on the temperature. A gasochromic change of more than 60% in transmittance at room temperature was observed, and the 90% response time was about 10 s at 25 °C, whereas the bleaching time was slower. Decreasing the

temperature led to a lower gasochromic response, but a reasonable response was still observed at −40 °C. Baseline drift was clearly observed when the gasochromic device was repeatedly exposed to hydrogen below 0 °C, which was attributed to the accumulation of water or ice formed in the gasochromic reaction.

Luo *et al.* studied the poisoning and reactivation of Pt nanoparticles on the surface of a $WO_3$ nanowire film during gasochromic reactions.[103] When exposed to air, the Pt/$WO_3$ film became inactive, leading to a longer coloration time, which was mainly caused by the poisoning of Pt nanoparticles. After annealing the Pt/$WO_3$ nanowire film at 120 °C, the coloration time decreased from 200 to 50 s, which was almost the same as that of the freshly prepared sample. XPS analysis revealed that the Pt nanoparticles were oxidized when exposed to air, leading to the low rate of hydrogen molecule dissociation in the gasochromic coloration. After annealing at 120 °C in air, the desorption of oxygen from the surface of Pt nanoparticles and the bleaching reaction between the $WO_3$ nanowires and Pt nanoparticles both contributed to the removal of oxygen, leading to the recovery of the gasochromic activity of the Pt/$WO_3$ nanowire film.

Nishizawa and co-workers have recently developed a novel method of fabricating Pt/$WO_3$ films without heating.[63] A solution containing Pt nanoparticles, $WO_3$, and oxalic acid was spin-coated onto a glass substrate to obtain Pt/$WO_3$ films. The Pt nanoparticles were uniformly dispersed, and oxalic acid helped stabilize the Pt/$WO_3$ nanoparticles by the formation of metal-oxalate complexes. When exposed to hydrogen, the Pt-oxalate complexes decomposed, leading to the reduction of $Pt^{2+}$ to Pt. The Pt/$WO_3$ films exhibited good long-term durability.

### 3.3 Flexible fabrication of gasochromic devices

The combination of $WO_3$ with novel structures and noble metals contributes to the development of high-performance gasochromic nanomaterials, which can rapidly sense hydrogen at room temperature. However, because $WO_3$-based gasochromic materials are typically inorganic powders, it would be very difficult to directly use these nanomaterials in a hydrogen fueling station for the detection of hydrogen leakage. Therefore, the flexible fabrication of gasochromic materials into devices is necessary for their application.[104]

The flexible fabrication methods of $WO_3$ gasochromic films can be divided into two: vapor-phase-based method and liquid-phase-based method. The vapor-phase-based method includes physical vapor deposition and chemical vapor deposition (CVD).[75,103] High-quality, dense, homogeneous films can be prepared using these methods, but their fabrication costs are generally high. The dense $WO_3$ films usually possess obvious disadvantages with small specific surface area, slow response rate, and stress-concentration-induced cracking. The liquid-phase-based method includes sol–gel method, template method, hydrothermal/solvothermal method, electrochemical anodization, and electrodeposition method, whose fabrication costs are relatively low.[34,82,88,103] Porous $WO_3$ films with various crystallized features are generally obtained by liquid-phase-based method methods, which are effective for gas penetrations. Some of the aforementioned methods are introduced in the following section.

Yaacob *et al.* investigated the gasochromic performances of $WO_3$ films on various transparent substrates, including quartz, glass, indium-doped tin oxide (ITO), and fluorine-doped tin oxide (FTO) conductive glass.[105] Different substrates exhibited different surface properties, leading to different morphologies of $WO_3$ and thus different surface interactions with hydrogen. The sizes of $WO_3$ grains on different substrates varied depending on the substrates. Figure 12 shows SEM images of various substrates before and after the introduction of $WO_3$. The sizes of the substrates increased in the order of glass (15–50 nm) < quartz (30–80 nm) < ITO (30–130 nm) < FTO (80–250 nm), whereas the sizes of the $WO_3$ films on quartz and glass were 30–40 nm and those on ITO and FTO were 40–60 nm and 300–500 nm, respectively. When exposed to 1% hydrogen, the optical wavelength of the Pd/$WO_3$ films changed, with marked changes detected on the glass and ITO substrates. The dynamic responses of Pd/$WO_3$ films deposited on the substrates towards 0.06–1.0% hydrogen are shown in Figs. 12(a3–d3). Compared with the FTO substrate, the other substrates exhibited fast responses and marked optical changes towards $H_2$.

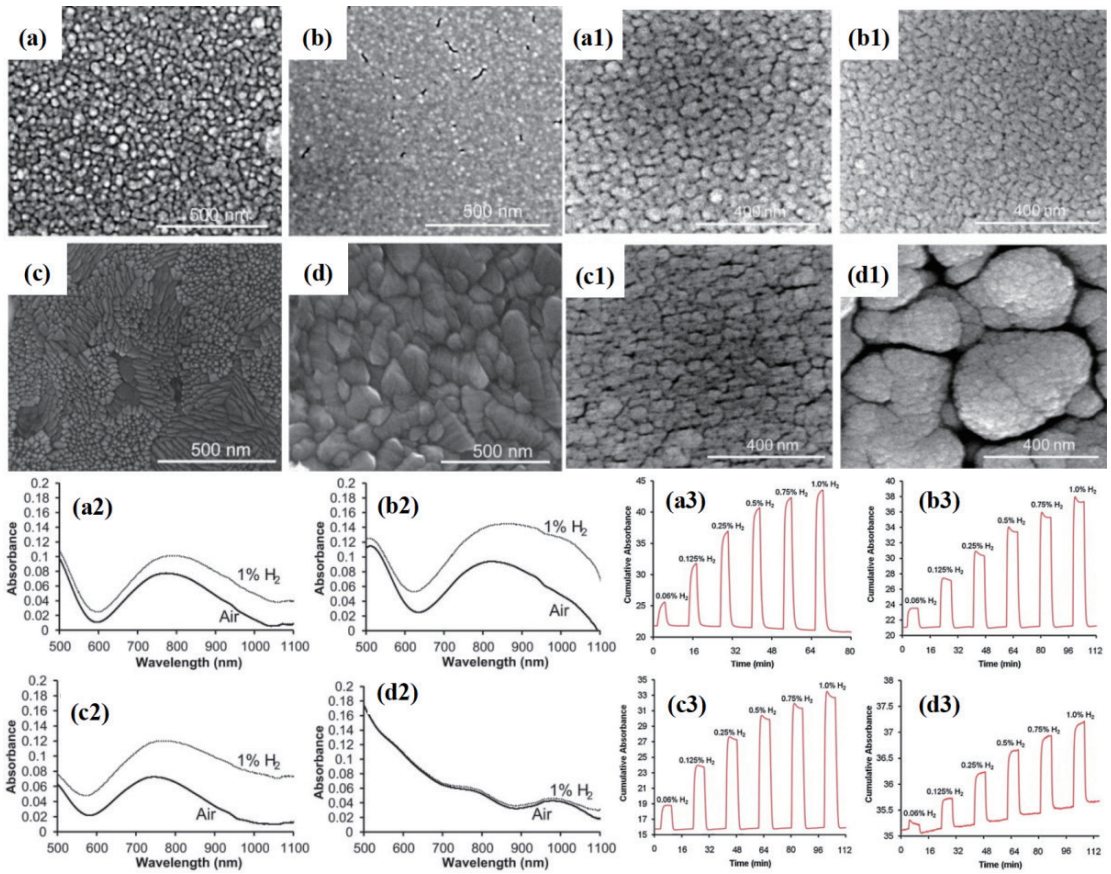


Fig. 12. (Color online) SEM images of surfaces of substrates of (a) quartz, (b) glass, (c) ITO, and (d) FTO. (a1–d1) SEM images of $WO_3$ thin films sputtered on the substrates in (a)–(d). (a2–d2) Absorbance vs optical wavelength of Pd/$WO_3$ films exposed to 1% $H_2$. (a3–d3) Dynamic performance of Pd/$WO_3$ thin films exposed to different $H_2$ concentrations. (Reprinted with permission from Ref. 105).

A transparent and flexible hydrogen gas sensor membrane was reported by Ishihara *et al.*[106] A Pt/$WO_3$ thin film was deposited on the surface of a polydimethylsiloxane (PDMS) membrane, which was pre-modified with hydroxyethyl acrylamide (HEAAm) by utilizing UV-light-induced graft polymerization. The PDMS membrane served as a substrate due to its gas permeability, high optical transparency, and cost-effectiveness. Upon introducing HEAAm, the PDMS surface changed from hydrophobic to hydrophilic; thus, a Pt/$WO_3$ film can be coated on the surface (Pt/$WO_3$-PDMS film). A gasochromic color change of the Pt/$WO_3$-PDMS film was observed after 300 s of exposure to 1.0 vol.% $H_2$ [Fig. 13(a)], and after heat treatment at 250 °C for 30 min, a color change was also detected, implying a high working temperature of the gasochromic membrane. The membrane of the Pt/$WO_3$-PDMS film exhibited high transparency and flexibility [Fig. 13(b)], and the scheme of this membrane is depicted in Fig. 13(c).

Owing to the 3D or 2D cross-linked structure, the preparation of a flexible gasochromic $WO_3$ film remains challenging because it would crack and be crushed during bending caused by internal stress. Therefore, a 1D or 0D structure of $WO_3$ with low cross-linkage is preferred. Edge-sharing $WO_3$ is reported to markedly decrease the cross-linkage.[77] Qi *et al.* proposed a

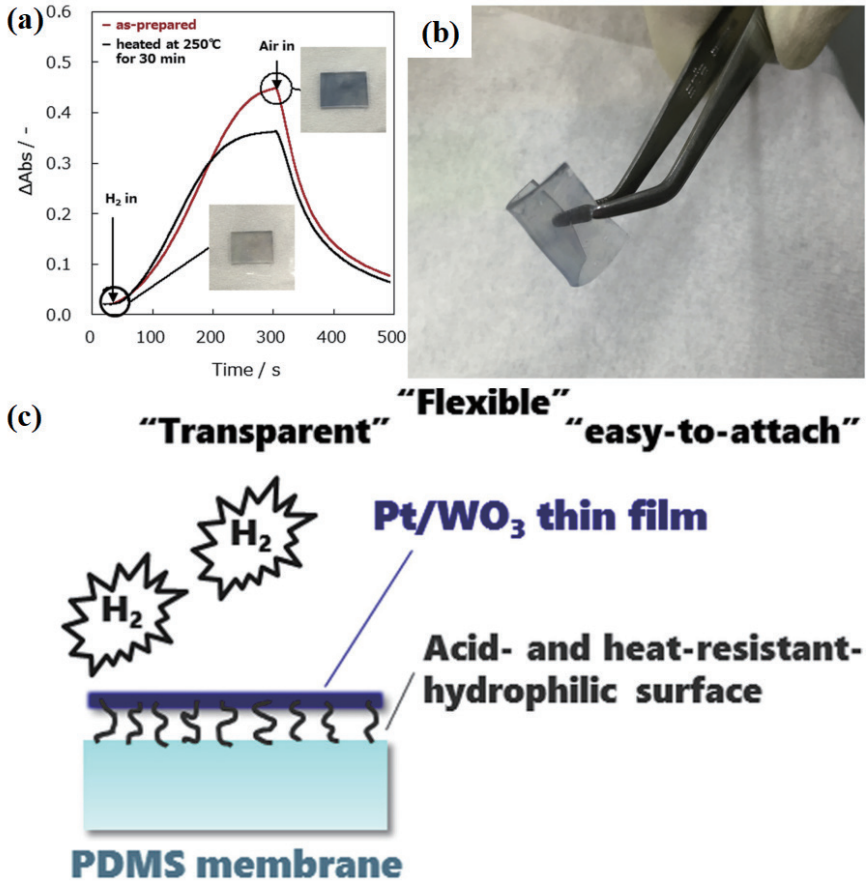


Fig. 13. (Color online) (a) Gasochromic hydrogen performance of Pt/$WO_3$-PDMS film. (b) Appearance and flexibility of Pt/$WO_3$-PDMS film. (c) Scheme of Pt/$WO_3$-PDMS film. (Reprinted with permission from Ref. 106).

photodeposition method of preparing a flexible edge-sharing $WO_3$ gasochromic film as shown in Fig. 14.[107] A tungsten solution was spin-coated on polyethylene terephthalate (PET). Then the as-prepared film was subjected to UV irradiation and finally dried [Fig. 14(a)]. The gasochromic performances of $WO_3$-PET films are shown in Figs. 14(b) and 14(c). The response times of the gasochromic cycles were very short. The initial coloration time of the $WO_3$-PET film after being exposed to $H_2$ was 20 s, and the bleaching time in an $O_2$ atmosphere was about 4 s. After 300 coloring/bleaching cycles, no marked decrease in the speed of the gasochromic reaction was detected. Figures 14(d) and 14(e) respectively show the $WO_3$-PET film before and after hydrogen injection in a flexibility test.

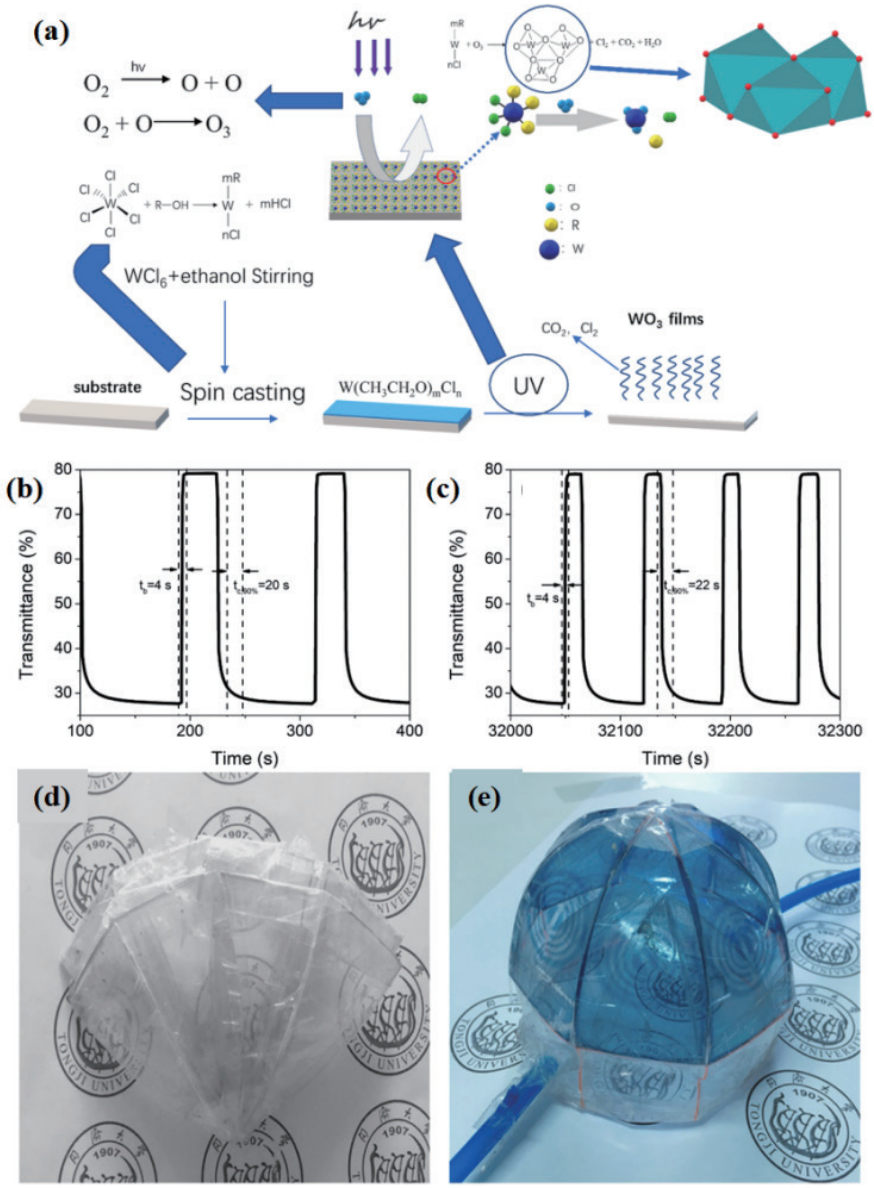


Fig. 14. (Color online) (a) Fabrication scheme of $WO_3$-PET film. (b) Initial results of cyclic tests of the $WO_3$-PET film and (c) results after 300 cycles. (d) and (e) $WO_3$-PET film before and after hydrogen injection, respectively. (Reprinted with permission from Ref. 107).

Lee *et al.* designed a very sensitive $H_2$ sensor that was easy to read by the eye, which consisted of a thin $WO_3$ film prepared by magnetron sputtering on a glass substrate and catalyzed by Pd through e-beam evaporation.[108] A cross-sectional SEM image of the $WO_3$ film on glass is shown in Fig. 15(a), and the estimated film thickness was about 610 nm. Figure 15(b) shows the porous structure of $WO_3$ with a gap of 5–10 nm. A PDMS coating was used to protect the hydrogen gasochromic device, which is shown in Fig. 15(c) and schematically shown in Fig. 15(d). After the introduction of PDMS, delays in gasochromic performances (coloring/bleaching times) towards $H_2$ were observed as shown in Fig. 15(e). Furthermore, the gasochromic performances of pure $H_2$ (10 sccm), pure $CH_4$ (10 sccm), mixed $H_2$+$CH_4$ (5:5 sccm), and mixed $H_2$+CO (5:5 sccm) were tested, and the results are shown in Fig. 15(f). Pure $CH_4$ showed no gasochromic activity, and CO served as a poison to the sensor, delaying the coloration. Enhanced gasochromic performance was observed in the $H_2$+$CH_4$ system. Figures 15(g) and 15(h) show photographic images of Pd/$WO_3$-PDMS sensors on a flexible substrate and on a hydrogen pipeline, respectively, before and after exposure to 1% $H_2$.

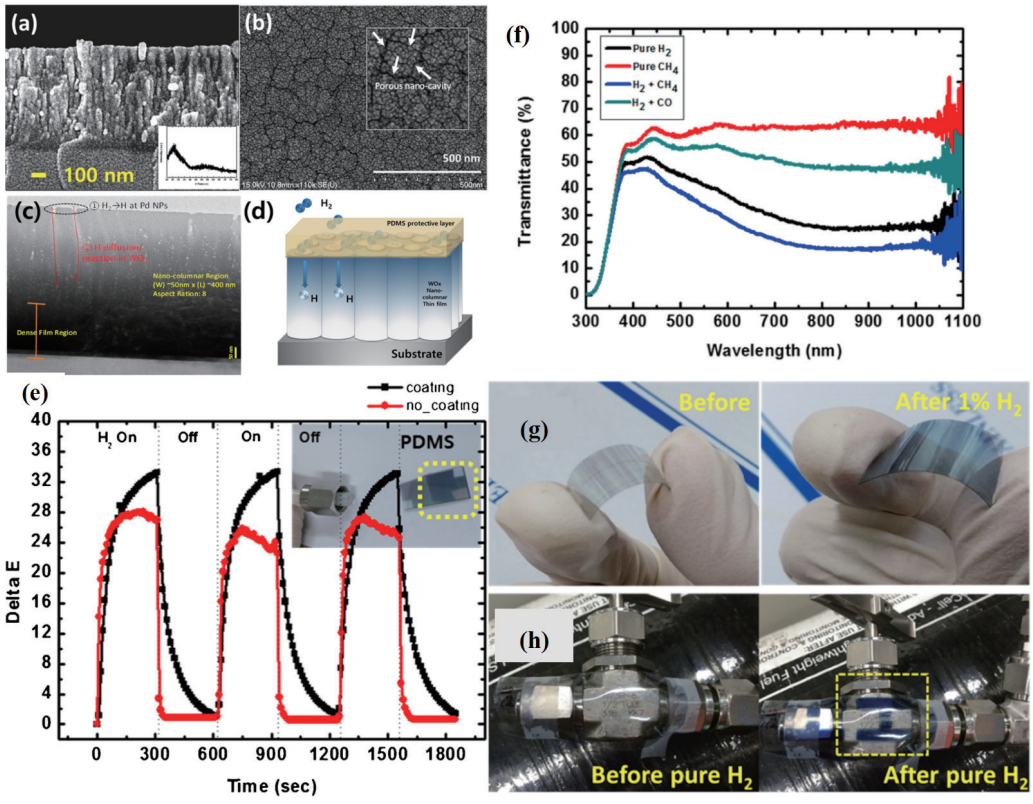


Fig. 15. (Color online) (a) SEM image and (b) surface plane view of $WO_3$. (c) Cross-sectional HRTEM image of $WO_x$ thin film. (d) Scheme of hydrogen diffusion along the $WO_x$ thin film. (e) Gasochromic cycling test of Pd/$WO_3$ on glass with and without PDMS coating. (f) Transmittance spectra under various gases. (g) Photographs of Pd/$WO_3$-PDMS sensors before and after exposure to 1% $H_2$. (h) Installation of Pd/$WO_3$-PDMS sensor on a pure $H_2$ pipeline. (Reprinted with permission from Ref. 108).

Ishihara *et al.* also used PDMS to obtain highly dispersed Pt/$WO_3$ gasochromic materials, thus realizing transparent and flexible hydrogen sensors.[37] After obtaining an optimized molar ratio of Pt/W of 1:13, they investigated the effects of the Pt/$WO_3$ content and heating temperature on hydrogen sensing performances. The results revealed that increasing the Pt/$WO_3$ nanoparticle content decreased transparency and led to a shorter coloration time. A membrane of 0.75 wt.% Pt/$WO_3$ nanoparticles exhibited enhanced gasochromic performances. High-temperature heating treatment resulted in the formation of crystalline Pt/$WO_3$ nanoparticles, inhibiting the access paths for hydrogen and increasing the gasochromic reaction time. An optimal heating temperature of 300 °C was found.

Zhang *et al.* synthesized a thick tungsten–silicon film with long-term gasochromic performance,[109] with methyltrimethoxysilane (MTMS) used as the Si source. The thickness of the $WO_3/SiO_2$ films increased to about 3 μm without any cracks [Figs. 16(a)–16(c)] with a concave region of 300–400 nm length. Figures 16(d) and 16(e) show the gasochromic performances of $WO_3/SiO_2$ films in colored/bleached states. A long cycle time was observed. Various gasochromic performances were detected for the $WO_3$-MTMS films with different ratios. When the ratio of MTMS to $WO_3$ was 0.1:1, the transmittance of the film in the colored/bleached states at 1000 nm was 60% and nearly 0%, respectively, and the gasochromic reaction time decreased with increasing number of cycles. When the ratio of $WO_3$/MTMS was 1:1, the transmittance of the bleached film from 900 to 1200 nm was lower than 2%, and performances of gasochromic cycles also decreased. Increasing the molar ratio of the $WO_3$/MTMS film to 1:2 led to high transmittance (67.5%) in the bleached state, and the film was colored in 25 s when it was first exposed to hydrogen.

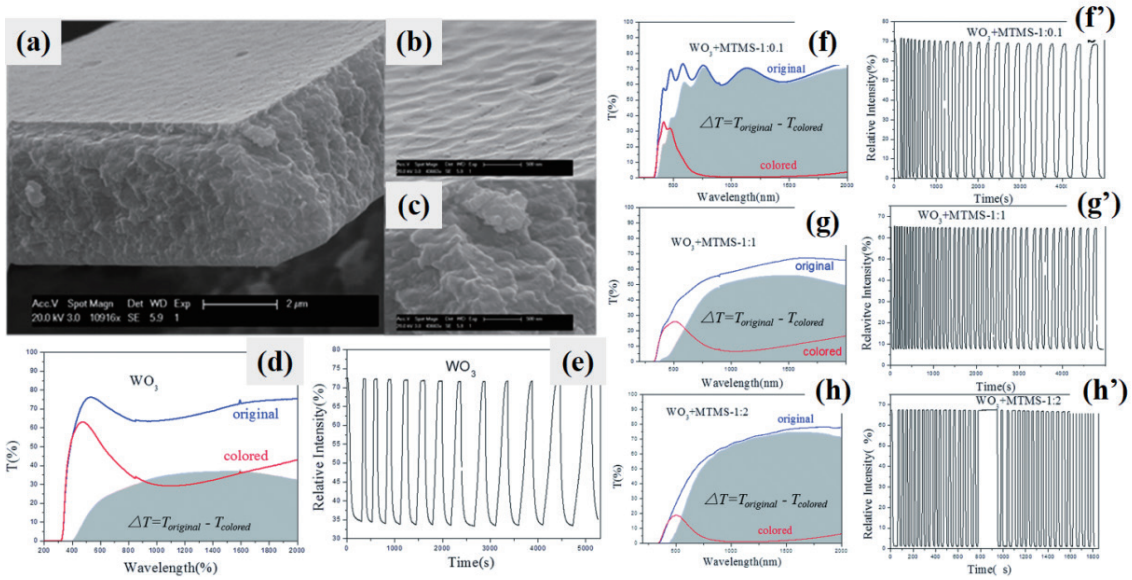


Fig. 16. (Color online) SEM images of (a) $WO_3$-MTMS compound film with 2 mm thickness, (b) surface of film, and (c) cross section. (d) Gasochromic properties of $WO_3/SiO_2$ films and (e) cycles of coloring/bleaching. (f–h) Gasochromic properties of $WO_3$-MTMS films with different ratios, and (f'–h') cycles of coloring/bleaching. (Reprinted with permission from Ref. 109).

Xue *et al.* proposed a novel strategy for manufacturing large-area gasochromic windows through an automated printing method.[43] By pre-hydrolyzing and condensing $SiO_2$, a $WO_3$/$SiO_2$ rheological ink was obtained, where the scheme is shown in Fig. 17(a). $WO_3$ and $SiO_2$ sols were first separately prepared then mixed with a molar ratio of 1:1. Three kinds of $SiO_2$, acid- ($tSiO_2$), alkali- ($aSiO_2$), and pre-hydrolyzed $SiO_2$ ($pSiO_2$), were prepared for comparison by using hydrochloric acid, ammonia, and deionized water, respectively. Nuclear magnetic resonance and DFT calculations revealed that the growth direction of $SiO_2$ depended on the pH value and that a neutral solution led to a porous $SiO_2$ network of satisfactory mechanical robustness, suitable rheological properties, and stable thermodynamics. The transmittance spectrum of the $WO_3$-$pSiO_2$ film is shown in Fig. 17(b). High transmittance was observed in the bleached state, whereas high absorptivity was detected in the colored state. The gasochromic performances of the three $WO_3$-$SiO_2$ films towards 10% $H_2$, showing the change in transmittance at 1000 nm, are exhibited in Fig. 17(c). After annealing at 100 °C, the gasochromic performances decreased [Fig. 17(d)]. Without high-temperature treatment, a gasochromic cycle was completed in 120 s for the three films, and with high-temperature treatment, the time was increased to 440 and 300 s for the $WO_3$-$tSiO_2$ and $WO_3$-$aSiO_2$ films, respectively. The $WO_3$-$aSiO_2$ film exhibited better gasochromic performances than the other films, which was attributed to the high porosity and uniform framework promoting the diffusion of hydrogen.

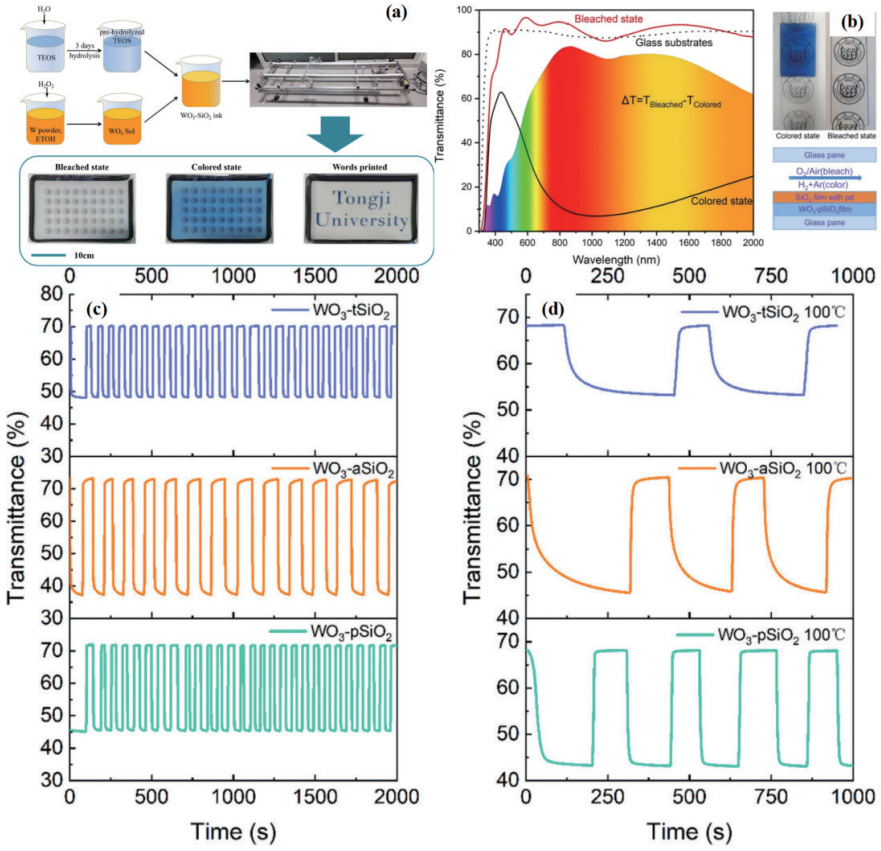


Fig. 17. (Color online) (a) Scheme of synthesis and auto-printing process for the $WO_3$-$pSiO_2$ ink. (b) Gasochromic tests of the $WO_3$-$pSiO_2$ films. (c) and (d) Gasochromic cycles for films before heat treatment and after heat treatment at 100 °C, respectively. (Reprinted with permission from Ref. 43).

Hu *et al.* prepared flexible Prussian blue/Pt (PB/Pt) nanocomposite gasochromic films by roll-to-roll (R2R) production,[110] the scheme of which is shown in Fig. 18(a). A flexible hydrophilic PET film was used as a substrate, and PB ink was first printed on PET by an R2R machine, then the Pt nanoparticles were deposited. The prepared Pt/PB/PET film is shown in Fig. 18(b). Owing to the hydrophobicity of the PB ink, hydroxypropyl cellulose (HPC) was added to the PB ink. The contact angles of PB ink droplets with various amounts of HPC are shown in Figs. 18(e)–18(h). For pure PB ink, the contact angle was 70.9°, meaning that it could not be directly used in the R2R process. After the introduction of 500, 1000, and 1500 ppm HPC, the contact angle decreased to 53.7, 53.0, and 51.7° immediately and further decreased to 51.7, 48.7, and 47.7° after 30 s, respectively. The gasochromic performances of the Pt/PB/PET films

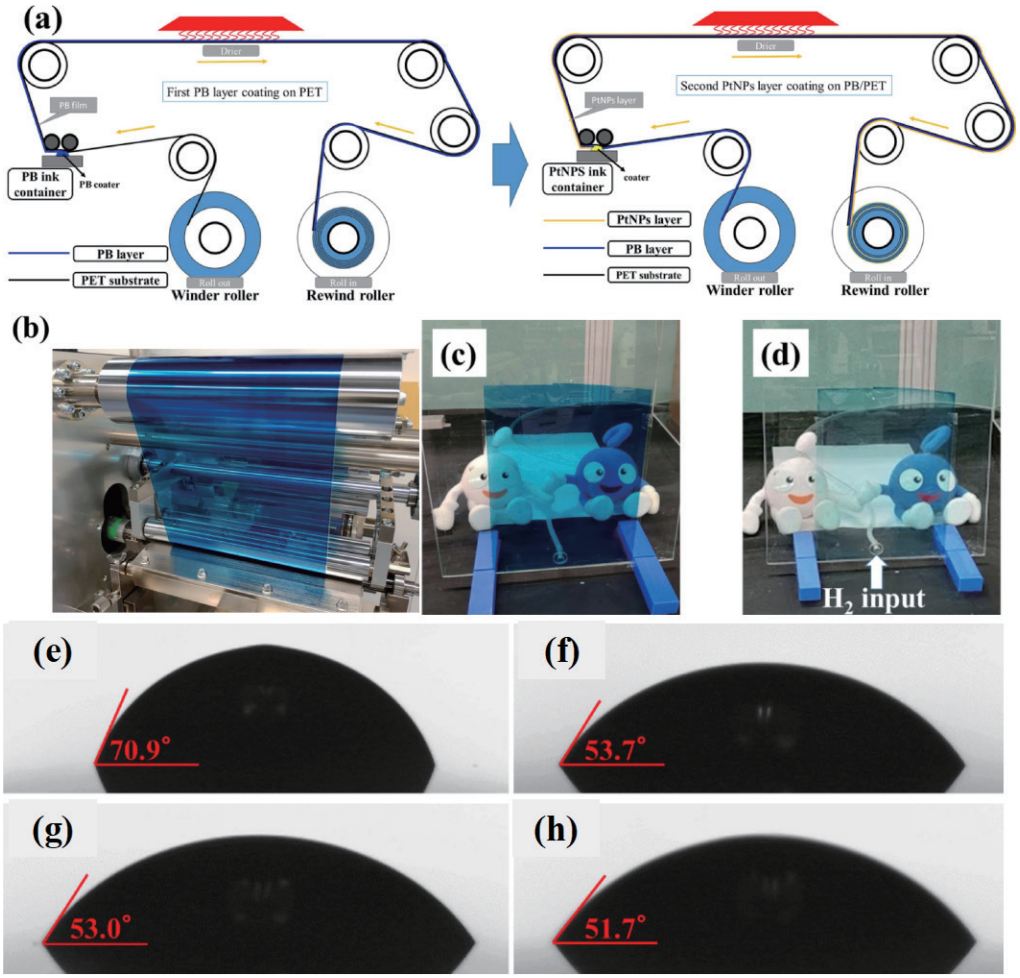


Fig. 18. (Color online) (a) Scheme of preparing PtNP/PB/PET film by R2R machine. (b) Image of the PB/PET film during manufacturing. (c) and (d) Images of the PB/PET film before and after hydrogen exposure. Contact angles of (e) pristine PB, (f) PB with 500, (g) PB with 1000, and (h) PB with 1500 ppm HPC. (Reprinted with permission from Ref. 110).

towards hydrogen showed a maximum change in transmittance of 77.8, 66.7, and 64.5% for the PB solution containing 500, 1000, and 1500 ppm HPC, respectively. Figures 18(c) and 18(d) show that the Pt/PB/PET film changed from blue to transparent after inputting hydrogen. Further attempts at the medium-scale production of gasochromic windows by sol–gel technology have been reported.[111] A window of 0.8 × 1.3 $m^2$ area has been prepared.

### 3.4. Non-$WO_3$-based gasochromic systems

Although $WO_3$-based gasochromic materials have been widely investigated, other materials, such as molybdenum oxides, vanadium oxides, and so forth, also exhibit gasochromic characteristics. Furthermore, some functional materials, including Y and NiOOH, exhibit unique optical changes when exposed to hydrogen. Therefore, non-$WO_3$-based gasochromic systems have been investigated, and typical results are briefly reviewed.

Dehaghi *et al.* prepared a Pd/$MoO_3$-coated polyester fabric for hydrogen detection.[112] A thin Pd film was first sputtered onto polyester fabric, then amorphous $MoO_3$ films were deposited by magnetron sputtering and the effect of the $O_2$/Ar ratio was investigated. SEM images of the polyester fabric, Pt-polyester fabric, and Pt/$MoO_3$-polyester fabric are shown in Fig. 19(a). The polyester fabric exhibited a fibrous morphology (about 10 μm thickness in the warp and weft dimensions). There was no obvious change after Pd introduction. However, the deposition of $MoO_3$ layers led to a rough surface. All the Pt/$MoO_3$-polyester fabric materials had a coloration time of about 4 min for different concentrations of hydrogen, whereas the recovery time was about 1–3 min upon exposure to 250 ppm hydrogen [Figs. 19(b) and 19(c)]. Further study will focus on obtaining a faster response.

Another limitation of the $MoO_3$-based gasochromic materials is a low bleaching rate compared with the $WO_3$-based gasochromic materials. Han *et al.* have recently solved this problem by using mixed-phase $MoO_3$ promoted by a multilayer Pt/Ni/Pi catalyst through e-beam evaporation.[65] The $MoO_3$ was composed of a- and b-phases, which were obtained by magnetron sputtering at 400 °C. The mixed-phase $MoO_3$ provided more active sites for reactions than a single phase (a- or b-phase). The thickness of the multilayer Pt/Ni/Pi catalyst was 4.5 nm, whereas that of the Ni layer was set to 0, 0.3, 0.5, 1.0, and 1.5 nm. The Ni layer promoted hydrogen dissociation by increasing the surface-to-volume ratio of Pt, which made the $MoO_3$ gasochromic materials exhibit reversible reactions. The $MoO_3$ film promoted by the Pt/Ni/Pi catalyst changed color from gray to navy blue within 30 s of hydrogen exposure and could be bleached within 50 s. In addition, a low detection limit of 5–1000 ppm $H_2$ was found in this system.

Kalanur *et al.* synthesized $MoO_3$ nanoplates by the hydrothermal method, where Pd nanoparticles were introduced through photochemical deposition, forming a room-temperature irreversible gasochromic sensor.[36] A full color change from white to blue was observed in 20 s upon exposure to pure hydrogen, and the gasochromic reaction times were about 4 and 7 min for 20% and 10% $H_2$, respectively. No color changes were observed for 1 and 0.1% hydrogen. XPS results revealed that the $MoO_3$ was reduced from $Mo^{6+}$ to $Mo^{5+}$ after the gasochromic reaction. Pd-modified $MoO_3$ nanowire labels were synthesized through a combination of the hydrothermal

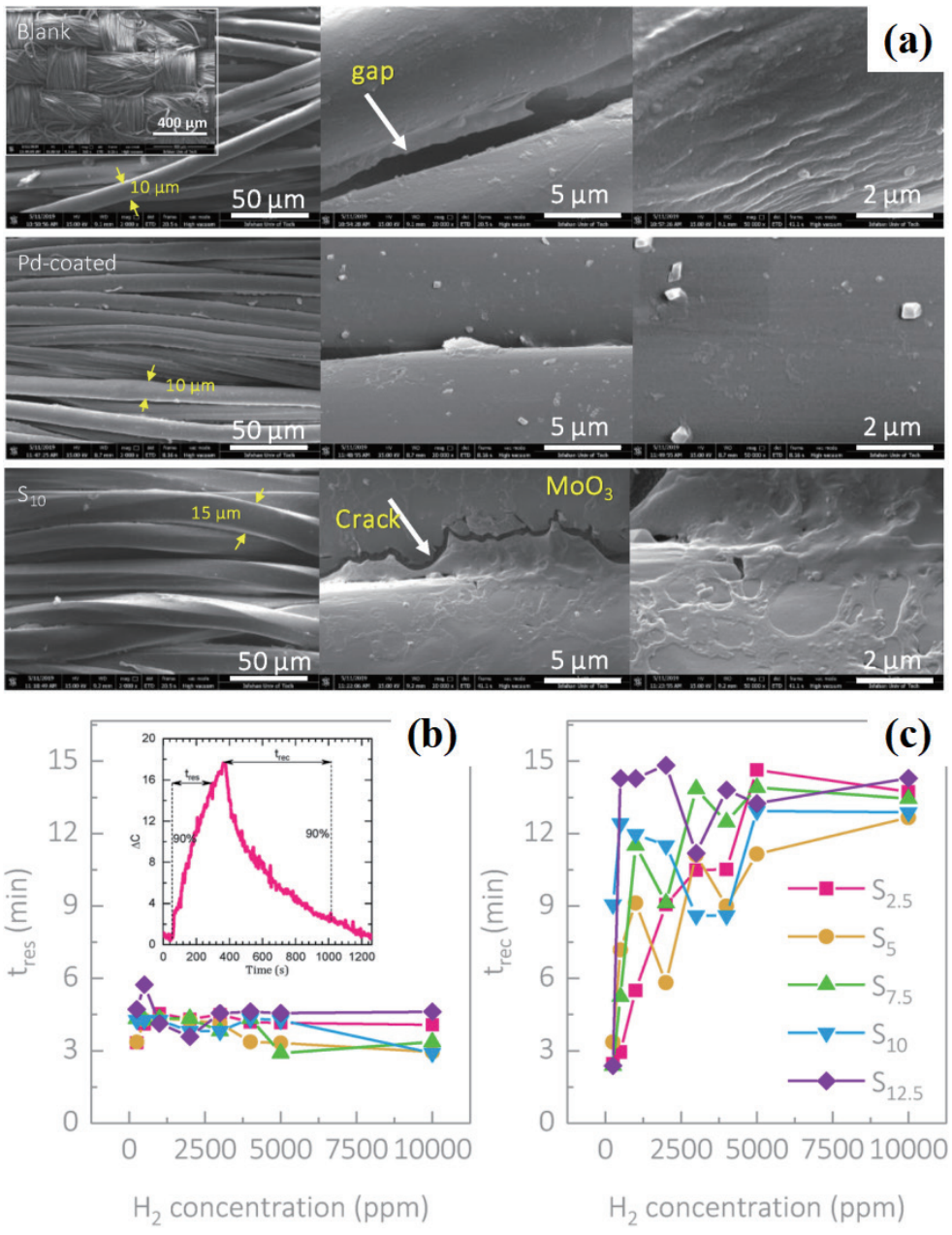


Fig. 19. (Color online) (a) SEM images of the Pt/$MoO_3$-polyester fabric material. (b) Response and (c) recovery time plots for various concentrations of $H_2$. (Reprinted with permission from Ref. 112).

method and self-assembly by Hu and co-workers.[64] An eye-readable color change from white to blue-gray occurred in 65 s, and the colored device bleached after heat treatment at 200 °C for 2 h. In the presence of other flammable gases, such as CO, $CH_3CH_2OH$, and $CH_3OH$, the gasochromic device showed high selectivity to hydrogen.

A hydrogen gas sensor based on Pd/$MoO_3$ nanobelts was prepared by Wang *et al.*[113] The $MoO_3$ nanobelts were prepared by the hydrothermal method, and the Pd/$MoO_3$ sensor was fabricated through spray deposition. A color change from light gray to dark blue that could be seen with the naked eye occurred in about 10 s for $H_2$ concentrations of as low as 1% $H_2$ at room temperature (Fig. 20), and the time was shortened to about 3 s when the sensor was exposed to pure hydrogen. The high $Mo^{5+}$ content in $MoO_3$ and the highly porous structure both contributed to the enhanced gasochromic activity.

Dong and Chen carried out a series of studies into the gasochromic behaviors and mechanisms of vanadium oxides. By controlling the spin-coating rate, a series of $V_2O_5$ films with various thicknesses were synthesized through the sol–gel method.[66] Gasochromic performances towards hydrogen were studied, and a color change from yellow to gray/black was observed. X-ray absorption spectroscopy (XAS) was used to reveal the gasochromic mechanism, and the results revealed that the introduction of hydrogen ions led to the partial reduction of vanadium (from $V^{5+}$ or $V^{4.8+}$ to $V^{4.1+}$) and that the structural symmetry of the $VO_6$ octahedron was distorted.[114] The local geometric and electronic structures of the gasochromic $VO_x$ films were studied,[115] and the effects of the oxygen partial pressure on the structural and gasochromic characters of $VO_x$ films were investigated.[116] The gasochromic mechanism, especially the changes in the structure and electrons on $VO_2$ film, were studied in depth.[117] Further research focused on the promotion of Mo-modified $V_2O_5$ films by Pt.[118] The results revealed that the

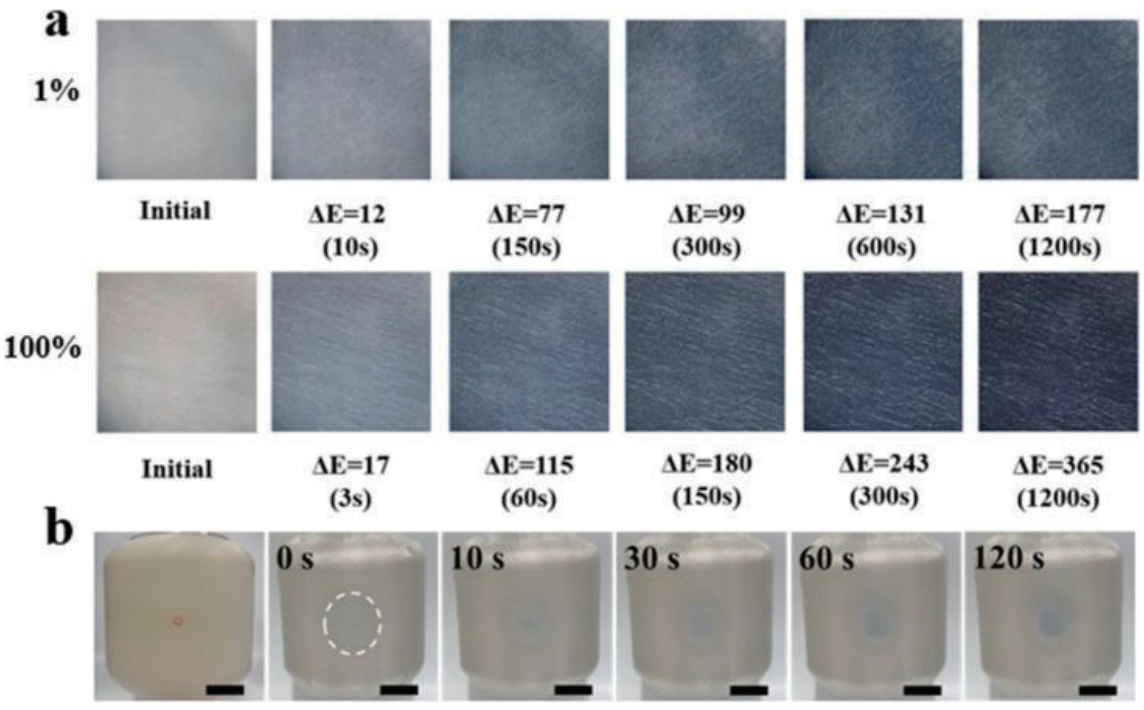


Fig. 20. (Color online) (a) Gasochromic photographs of Pd/$MoO_3$ sensors for hydrogen concentrations of 1 and 100%. (b) Sensor attached to a hydrogen storage tank for leakage detection (bar is 5 cm). (Reprinted with permission from Ref. 113).

introduction of Mo into a $V_2O_5$ film led to a more amorphous structure than that of the pristine $V_2O_5$ film. *In situ* soft- and hard-XAS analysis showed that the modification of a $V_2O_5$ film by Mo atoms led to a mixture of pyramid- and octahedral-like structures, whereas there was a pyramid-like oxygen-coordinated environment for a pure $V_2O_5$ film (Fig. 21). During the gasochromic reaction, the adsorption of hydrogen added electrons to the 3d $t_{2g}$ orbital of the V atoms and lowered their charge state.

Chandra's group developed a Pd/$V_2O_5$ film for hydrogen sensing by magnetron reactive sputtering.[119] The gasochromic performances of the Pd/$V_2O_5$ film were investigated by spectroscopic ellipsometry, and the formation of vanadium bronze was detected, which was attributed to the gasochromic behavior.

Ngene and co-workers reported a novel optical hydrogen detector composed of a Pd-capped Y thin film.[120,121] The structure of the device is shown in Fig. 22(a). Quartz was used as a substrate. The sensing layer was a thin film of Y ranging in thickness from 30 to 150 nm. Pd and polytetrafluoroethylene (PTFE) layers with thicknesses of 50 and 30 nm, respectively, served as a (de-)hydrogenation catalyst and as protection from deterioration, respectively. Another catalyst layer of $Pd_xAu_{1-x}$ was also prepared.[40] After exposure to hydrogen, the Y formed a semitransparent $YH_2$ phase at 10–31 mbar and $YH_3$ at 0.1 mbar. Various colors were observed due to reflection differences between the substrate/$Yh_x$ and $Yh_x$/Pd interfaces. Further changing the thickness of the Y thin films affected the interfaces and tuned the colors of the hydrogen detectors.

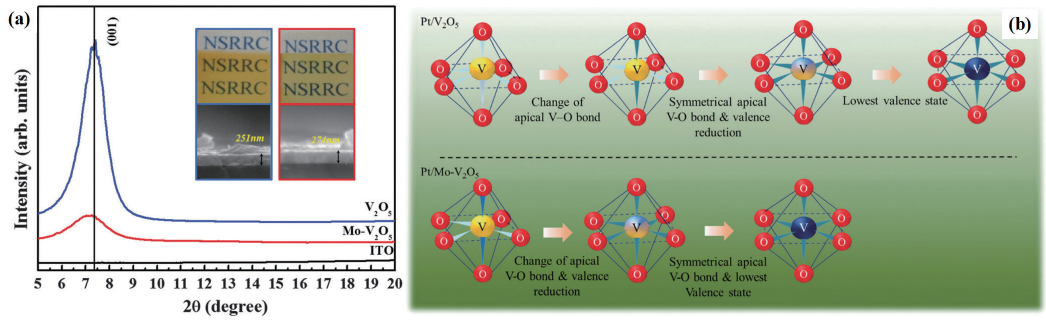


Fig. 21. (Color online) (a) XRD patterns and (b) gasochromic coloration of Mo-modified $V_2O_5$ thin films. (Reprinted with permission from Ref. 118).

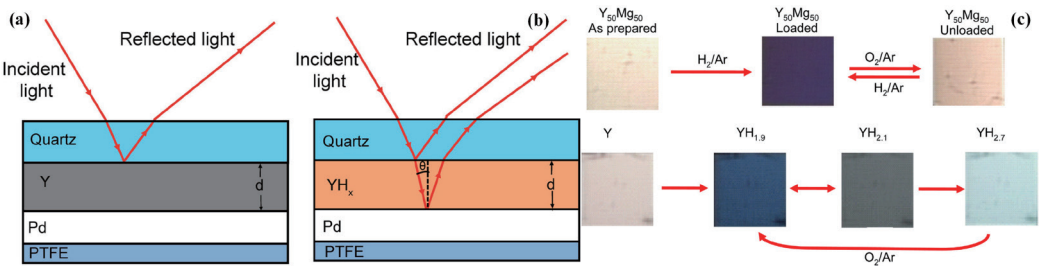


Fig. 22. (Color online) (a) Scheme and (b) color changes of Y-based gasochromic material. (Reprinted with permission from Refs. 120 and 121).

Hu *et al.* synthesized a nickel oxyhydroxide (NiOOH) thin film by chemical bath deposition, then they sputtered a Pd catalyst layer onto the NiOOH thin film to fabricate a novel NiOOH/Pd device for hydrogen detection,[122] as illustrated in Fig. 23(a). The NiOOH/Pd gasochromic device exhibited two unique properties. First, it changed from black to transparent when exposed to hydrogen, especially at 650 and 550 nm, with transmittances of 50.6% and 47%, respectively [Fig. 23(b)]. Second, a memory effect was observed in the NiOOH thin film, which allowed the colored/bleached states to be maintained for more than 21 days before/after hydrogen exposure. When applying an electrochemical process (0.6 V), the NiOOH/Pd device changed from transparent to black. Further research has focused on the introduction of Pd nanoparticles and the bleaching method,[123] where the as-synthesized Pd nanoparticles were mixed with NiOOH, thus obtaining a NiOOH/Pd complex, and $O_3$ was used to bleach the color of the NiOOH/Pd device.

Another eye-readable gasochromic hydrogen gas sensor derived from CuS-Pd was reported by Seo *et al.*[35] An ultrathin CuS film was deposited by chemical bath deposition, and a Pd layer was deposited through electron beam deposition. An eye-readable color change from dark green to brown was observed when the CuS-Pd film was exposed to hydrogen. This CuS film can detect as low as 0.8% hydrogen in air.

A novel gasochromic sensor based on Pd-decorated PdO nanoparticle nanonetworks (Pd-PdO NNs) has also been proposed.[124] In this sensor, the reduction of PdO with hydrogen was an auto-catalytic reaction, which was promoted by Pd species.[125] A color change from brown yellow to gray was observed after exposure to hydrogen, while the final color depended on the concentration of hydrogen [Fig. 24(a)]. The gasochromic mechanism is shown in Fig. 24(b), which includes the activation of hydrogen by Pd and a gasochromic reaction between PdO and active hydrogen species.

Recently, Mandel *et al.* have reported novel supraparticles (SPs) for gasochromic hydrogen detection.[126] These SPs were composed of spray-dried $SiO_2$ nanoparticles, Au-Pd nanoparticles, and the indicator dye resazurin. After exposure to hydrogen, the SPs irreversibly changed from purple to pink, then reversibly to a colorless state (Fig. 25). A study of the mechanism revealed that the two-step color changes were due to the reduction of resazurin to resorufin and then to hydroresorufin.

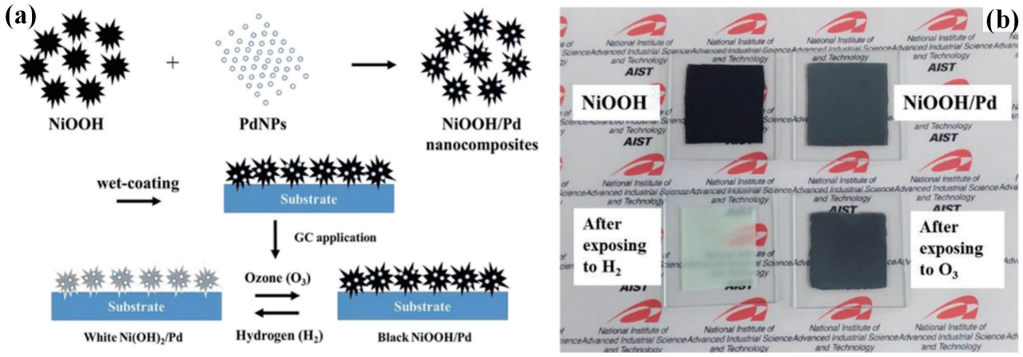


Fig. 23. (Color online) (a) Scheme of synthesizing NiOOH/Pd device and (b) gasochromic performance. (Reprinted with permission from Ref. 122).

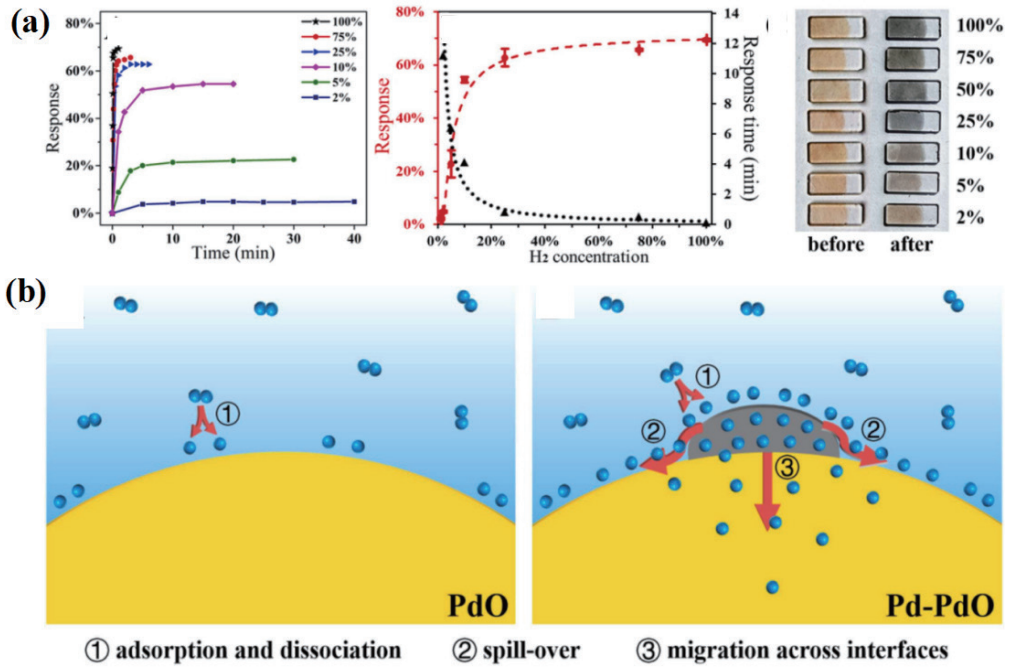


Fig. 24. (Color online) (a) Gasochromic performances of Pd-PdO NNs and (b) reaction mechanism. (Reprinted with permission from Ref. 124).

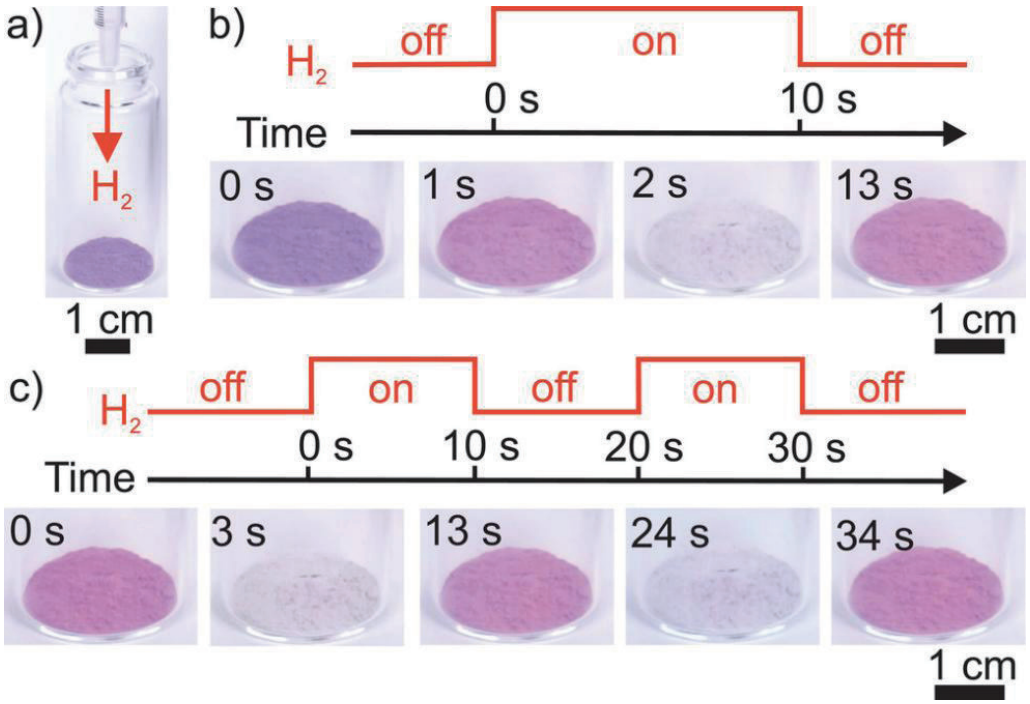


Fig. 25. (Color online) Color changes of the SPs during various stages. (a) Setup for the functional characterization; (b) snapshots of the color-change reaction of the SP powder when exposed to a defined $H_2$ exposure program for the first time and (c) upon repeated exposure. (Reprinted with permission from Ref. 126).

In addition to the gasochromic transition metal oxides, some organic compounds and mixed metal oxides also exhibit similar properties, such as Pt-nanoparticle-decorated poly(3,4-alkylenedioxythiophenes),[127] polyaniline polystyrene sulfonate/platinum nanoparticles,[128] Prussian blue/Pt nanoparticles,[129] $(WO_3)_{1-x}(V_2O_5)_x$,[130] and $TiO_2/WO_3$.[131]

## 4. Perspectives

The development of hydrogen infrastructure is of great importance in realizing a zero-emission and clean society, in which hydrogen safety will play a vital role. This technical paper focuses on hydrogen leakage detection based on gasochromic reactions. It also reviews gasochromic mechanisms and state-of-the-art research, including on the preparation of $WO_3$ with novel structures, noble metals to promote reactions, the flexible fabrication of gasochromic devices, and non-$WO_3$-based gasochromic systems. Considering the urgent need for hydrogen development, more efforts should be paid to achieve the tough targets set by DOE, including dynamic range and detection limit both <4 vol.%, response/recovery times both <30 s, and price ≤$40 per unit for stationary applications. Several perspectives on gasochromic research are proposed as follows.

First, regarding the gasochromic mechanism, advanced techniques, especially *in situ* real-time techniques, should be adopted to reveal the structural, electrical, and optical changes in gasochromic nanomaterials. Moreover, the isotope labeling of several elements, such as W, O, and H, can contribute to clarifying the reaction pathways. In addition, more attention should be focused on the behavior of hydrogen in coloring/bleaching.

Second, because $WO_3$ is a widely investigated gasochromic material, we suggest focusing on the design of $WO_3$ with specific phases, morphologies, facets, and other physiochemical properties. This will contribute to discovering gasochromic nanomaterials with enhanced performance. In addition, $WO_3$ with specific properties will help reveal the reaction mechanisms. Furthermore, attempts to explore novel non-$WO_3$-based gasochromic nanomaterials should be encouraged, especially through the combination of various materials.

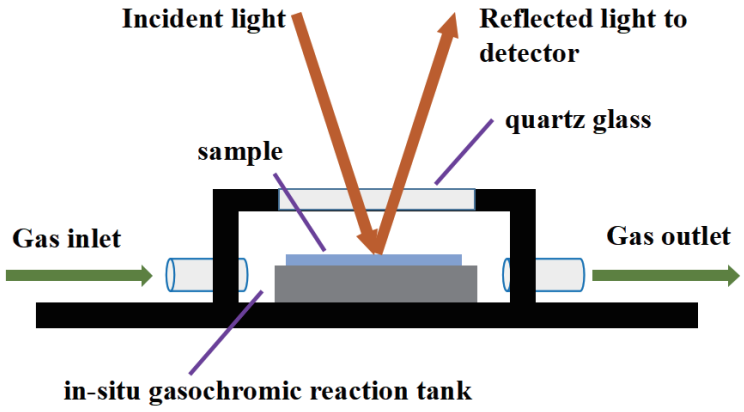


Fig. 26. (Color online) Potential scheme for gasochromic performance tests.

Third, referring to flexible fabrication, more attention should be focused on practical applications. It is vital to fabricate gasochromic devices suitable for various hydrogen-related circumstances, such as hydrogen production, delivery, storage, and usage. Moreover, the effects of environmental factors, such as temperature, humidity, and UV light, should be considered.

Finally, an urgent task is to establish a standard method for evaluating gasochromic performances. To be more specific, the gasochromic activities of various nanomaterials should be measured by a method in which, for example, the shapes and sizes of the *in situ* reaction tank, the flow directions and pipe diameters of the hydrogen flow, the measurements of optical changes, and so forth, are standardized. A potential scheme for gasochromic performance tests is proposed in Fig. 26. This will allow gasochromic rates in various studies to be compared.

## Acknowledgments

This work was supported by Sinopec Group under Grant 321140.

## References

1 C. Acar and I. Dincer: Int. J. Hydrogen Energy. **45** (2020) 3396. https://doi.org/10.1016/j.ijhydene.2018.10.149
2 W. T. Koo, H. J. Cho, D. H. Kim, Y. H. Kim, H. Shin, R. M. Penner, and I. D. Kim: ACS Nano **14** (2020) 14284. https://doi.org/10.1021/acsnano.0c05307
3 M. Yue, H. Lambert, E. Pahon, R. Roche, S. Jemei, and D. Hissel: Renewable Sustainable Energy Rev. **146** (2021) 111180. https://doi.org/10.1016/j.rser.2021.111180
4 J. Sui, Z. Chen, C. Wang, Y. Wang, J. Liu, and W. Li: Appl. Energy **276** (2020) 115409. https://doi.org/10.1016/j.apenergy.2020.115409
5 N. Muradov: Int. J. Hydrogen Energy **42** (2017) 14058. https://doi.org/10.1016/j.ijhydene.2017.04.101
6 Z. Li, P. Guo, R. Han, and H. Sun: Energy Explor. Exploit. **37** (2018) 5. https://doi.org/10.1177/0144598718787294
7 D. Jang, K. Kim, K.-H. Kim, and S. Kang: Energy Convers. Manage. **263** (2022) 115695. https://doi.org/10.1016/j.enconman.2022.115695
8 T. Kowalczyk, J. Badur, and M. Bryk: Energy Convers. Manage. **198** (2019) 111805. https://doi.org/10.1016/j.enconman.2019.111805
9 H. M. El-Bery, and H. N. Abdelhamid: J. Environ. Chem. Eng. **9** (2021) 105702. https://doi.org/10.1016/j.jece.2021.105702
10 Z. Y. Yu, Y. Duan, X. Y. Feng, X. Yu, M. R. Gao, and S. H. Yu: Adv. Mater. **33** (2021) 2007100. https://doi.org/10.1002/adma.202007100
11 E. Ogungbemi, T. Wilberforce, O. Ijaodola, J. Thompson, and A. G. Olabi: Int. J. Hydrogen Energy **46** (2021) 30625. https://doi.org/10.1016/j.ijhydene.2020.06.147
12 A. Ajanovic and R. Haas: Int. J. Hydrogen Energy **46** (2021) 10049. https://doi.org/10.1016/j.ijhydene.2020.03.122
13 M. Molnarne and V. Schroeder: Process Saf. Environ. Prot. **130** (2019) 1. https://doi.org/10.1016/j.psep.2019.07.012
14 X. T. Yin, S. S. Wu, D. Dastan, S. Nie, Y. Liu, Z. G. Li, Y. W. Zhou, J. Li, A. Faik, K. Shan, Z. Shi, M. A. Tarighat, and X. G. Ma: Surf. Interfaces **25** (2021) 101190. https://doi.org/10.1016/j.surfin.2021.101190
15 M. Hirayama, H. Shinozaki, N. Kasai, and T. Otaki: Int. J. Hydrogen Energy **43** (2018) 12584. https://doi.org/10.1016/j.ijhydene.2018.05.003
16 C. Zhou, Y. Song, Q. Shi, S. Hu, J. Zheng, P. Xu, and L. Zhang: Int. J. Hydrogen Energy **44** (2019) 26036. https://doi.org/10.1016/j.ijhydene.2019.08.046
17 C. Colombo, A. Zafra García, J. Belzunce, and I. Fernandez Pariente: Theor. Appl. Fract. Mech. **110** (2020) 102810. https://doi.org/10.1016/j.tafmec.2020.102810
18 X. Liu, X. Chen, J. Ju, X. Wang, Z. Mei, H. Qu, Y. Xu, and X. Zeng: ACS Appl. Nano Mater. **2** (2019) 2958. https://doi.org/10.1021/acsanm.9b00380
19 Q. A. Drmosh and Z. H. Yamani: Ceram. Int. **42** (2016) 12378. https://doi.org/10.1016/j.ceramint.2016.05.011
20 D. Zhang, Y. Sun, C. Jiang, and Y. Zhang: Sens. Actuators, B **242** (2017) 15. https://doi.org/10.1016/j.snb.2016.11.005

21 X. Chi, X. Wang, X. Ke, and X. Zhang: IEEE Photonics Technol. Lett. **34** (2022) 687. https://doi.org/10.1109/LPT.2022.3181676
22 A. Mirzaei, J. H. Kim, H. W. Kim, and S. S. Kim: Appl. Sci. **9** (2019) 1775. https://doi.org/10.3390/app9091775
23 M. O. Kim, K. Lee, H. Na, D. S. Kwon, J. Choi, J. I. Lee, D. H. Baek, and J. Kim: Sens. Actuators, B **197** (2014) 414. https://doi.org/10.1016/j.snb.2014.03.019
24 J. Wu, Y. Guo, Y. Wang, H. Zhu, and X. Zhang: Sens. Actuators, B **361** (2022) 131693. https://doi.org/10.1016/j.snb.2022.131693
25 D. Sil, J. Hines, U. Udeoyo, and E. Borguet: ACS Appl. Mater. Interfaces **7** (2015) 5709. https://doi.org/10.1021/am507531s
26 B. Ai, Y. Sun, and Y. Zhao: Small **18** (2022) 2107882. https://doi.org/10.1002/smll.202107882
27 G. Wang, J. Dai, and M. Yang: IEEE Sens. J. **21** (2021) 12706. https://doi.org/10.1109/JSEN.2020.3029519
28 K. Chen, D. Yuan, and Y. Zhao: Opt. Laser Technol. **137** (2021) 106808. https://doi.org/10.1016/j.optlastec.2020.106808
29 H. S. Lee, J. Kim, H. Moon, and W. Lee: Adv. Mater. **33** (2021) 2005929. https://doi.org/10.1002/adma.202005929
30 J. Ajayan, D. Nirmal, R. Ramesh, S. Bhattacharya, S. Tayal, L. M. I. Leo Joseph, L. Raju Thoutam, and D. Ajitha: Measurement **186** (2021) 110100. https://doi.org/10.1016/j.measurement.2021.110100
31 I. Darmadi, F. A. Nugroho, and C. Langhammer: ACS Sens. **5** (2020) 3306. https://doi.org/10.1021/acssensors.0c02019
32 A. V. Almaev, V. I. Nikolaev, N. N. Yakovlev, P. N. Butenko, S. I. Stepanov, A. I. Pechnikov, M. P. Scheglov, and E. V. Chernikov: Sens. Actuators, B **364** (2022) 131904. https://doi.org/10.1016/j.snb.2022.131904
33 S. Chen, J. Luo, H. Tan, J. Chen, S. Deng, and N. Xu: Sens. Actuators, B **173** (2012) 824. https://doi.org/10.1016/j.snb.2012.07.120
34 S. Cho, J. Suh, B. Jeong, T. Lee, K. Choi, T. Eom, T. Kim, and H. Jang: Chem. Eng. J. **446** (2022) 136862. https://doi.org/10.1016/j.cej.2022.136862
35 S. S. Kalanur, Y. A. Lee, and H. Seo: RSC Adv. **5** (2015) 9028. https://doi.org/10.1039/c4ra11067f
36 S. Kalanur, I. Yoo, and H. Seo: Sens. Actuators, B **247** (2017) 357. https://doi.org/10.1016/j.snb.2017.03.033
37 R. Ishihara, Y. Makino, Y. Yamaguchi, K. Fujimoto, and K. Nishio: Membranes **12** (2022) 291. https://doi.org/10.3390/membranes12030291
38 S. Zhang, H. Li, and Z. Yang: J. Alloys Compd. **722** (2017) 555. https://doi.org/10.1016/j.jallcom.2017.06.095
39 H. Yang, H. Sun, Q. Li, P. Li, K. Song, B. Song, and L. Wang: Vacuum. **164** (2019) 411. https://doi.org/10.1016/j.vacuum.2019.03.053
40 P. Ngene, R. J. Westerwaal, S. Sachdeva, W. Haije, L. C. P. M. de Smet, and B. Dam: Angew. Chem. Int. Ed. **53** (2014) 12081. https://doi.org/10.1002/anie.201406911
41 C. V. Ramana, S. Utsunomiya, R. Ewing, C. Julien, and U. Becker: J. Phys. Chem. B **110** (2006) 10430. https://doi.org/10.1021/jp056664i
42 J. Lee, H. Koo, S. Y. Kim, S. J. Kim, and W. Lee: Sens. Actuators, B **327** (2021) 128930. https://doi.org/10.1016/j.snb.2020.128930
43 S. Xue, G. Gao, Z. Zhang, X. Jiang, J. Shen, G. Wu, H. Dai, Y. Xu, and Y. Xiao: ACS Appl. Nano Mater. **4** (2021) 8368. https://doi.org/10.1021/acsanm.1c01557
44 J. Li, C. Guo, L. Li, Y. Gu, B. Kim, and J. Huang: RSC Adv. **11** (2021) 23700. https://doi.org/10.1039/d1ra03149j
45 L. Kong, X. Guo, J. Xu, Z. Mo, and L. Li: J. Photochem. Photobiol., A **401** (2020) 112760. https://doi.org/10.1016/j.jphotochem.2020.112760
46 F. Zheng, W. Man, M. Guo, M. Zhang, and Q. Zhen: CrystEngComm **17** (2015) 5440. https://doi.org/10.1039/c5ce00832h
47 F. Tavakoli Foroushani, H. Tavanai, M. Ranjbar, and H. Bahrami: Sens. Actuators, B **268** (2018) 319. https://doi.org/10.1016/j.snb.2018.04.120
48 A. Boudiba, C. Zhang, P. Umek, C. Bittencourt, R. Snyders, M.-G. Olivier, and M. Debliquy: Int. J. Hydrogen Energy. **38** (2013) 2565. https://doi.org/10.1016/j.ijhydene.2012.11.040
49 J. Zhou, S. Lin, Y. Chen, and A. Gaskov: Appl. Surf. Sci. **403** (2017) 274. https://doi.org/10.1016/j.apsusc.2017.01.209
50 N. Lu, X. Gao, C. Yang, F. Xiao, J. Wang, and X. Su: Sens. Actuators, B **223** (2016) 743. https://doi.org/10.1016/j.snb.2015.09.156
51 P. Ou, F. Song, Y. Yang, J. Shao, Y. Hua, S. Yang, H. Wang, Y. Luo, and J. Liao: ACS Omega **7** (2022) 8833. https://doi.org/10.1021/acsomega.1c07147
52 Z. Wang, D. Chu, L. Wang, L. Wang, W. Hu, X. Chen, H. Yang, and J. Sun: Appl. Surf. Sci. **396** (2017) 492. https://doi.org/10.1016/j.apsusc.2016.10.181

53 C. Wu, Z. Zhu, S. Huang, and R. Wu: J. Alloys Compd. **776** (2019) 965. https://doi.org/10.1016/j.jallcom.2018.10.372
54 C. Song, G. Wu, B. Sun, Y. Xiong, S. Zhu, Y. Hu, H. Gu, Y. Wang, and W. Chen: Int. J. Hydrogen Energy **42** (2017) 6420. https://doi.org/10.1016/j.ijhydene.2016.12.101
55 Z. Liu, B. Liu, W. Xie, H. Li, R. Zhou, Q. Li, and T. Wang: Sens. Actuators, B **235** (2016) 614. https://doi.org/10.1016/j.snb.2016.05.140
56 S. Wei, S. Li, R. Wei, S. Liu, and W. Du: Sens. Actuators, B **329** (2021) 129188. https://doi.org/10.1016/j.snb.2020.129188
57 C. Wang, Y. Zhang, X. Sun, Y. Sun, F. Liu, X. Yan, C. Wang, P. Sun, and G. Lu: Sens. Actuators, B **321** (2020) 128629. https://doi.org/10.1016/j.snb.2020.128629
58 M. Punginsang, D. Zappa, E. Comini, A. Wisitsoraat, G. Sberveglieri, A. Ponzoni, and C. Liewhiran: Appl. Surf. Sci. **571** (2022) 151262. https://doi.org/10.1016/j.apsusc.2021.151262
59 S. Zhao, Y. Shen, P. Zhou, X. Zhong, C. Han, Q. Zhao, and D. Wei: Sens. Actuators, B **282** (2019) 917. https://doi.org/10.1016/j.snb.2018.11.142
60 W. Song, R. Zhang, X. Bai, Q. Jia, and H. Ji: J. Mater. Sci.: Mater. Electron. **31** (2019) 610. https://doi.org/10.1007/s10854-019-02565-6
61 S. Li, A. Liu, Z. Yang, L. Zhao, J. Wang, F. Liu, R. You, J. He, C. Wang, X. Yan, P. Sun, X. Liang, and G. Lu: Sens. Actuators, B **289** (2019) 252. https://doi.org/10.1016/j.snb.2019.03.073
62 S. Okazaki and S. Johjima: Thin Solid Films **558** (2014) 411. https://doi.org/10.1016/j.tsf.2014.02.080
63 K. Nishizawa, C.-W. Hu, and Y. Yamada: Sol. Energy Mater. Sol. Cells **245** (2022) 111891. https://doi.org/10.1016/j.solmat.2022.111891
64 K. You, F. Cao, G. Wu, P. Zhao, H. Huang, Z. Wang, Y. Hu, H. Gu, and J. Wang: Mater. Chem. Phys. **227** (2019) 111. https://doi.org/10.1016/j.matchemphys.2019.01.070
65 S. I. Han, S. Y. Lee, L. T. Duy, and H. Seo: Int. J. Hydrogen Energy **46** (2021) 33339. https://doi.org/10.1016/j.ijhydene.2021.07.091
66 Y. Ho, C. Chang, D. Wei, C. Dong, C. Chen, J. Chen, W. Jang, C. Hsu, T. Chan, K. Kumar, C. Chang, and M. Wu: Thin Solid Films **544** (2013) 461. https://doi.org/10.1016/j.tsf.2013.02.080
67 Y. Lu, H. Hsu, J. Chen, H. Chang, C. Chen, W. Choud, C. Dong: Phys. Chem. Chem. Phys. **18** (2016) 5203. https://doi.org/10.1039/c5cp06870c
68 A. Georg, W. Neumann, and V. Wittwer: Solid State Ionics **127** (2000) 319. https://doi.org/10.1016/s0167-2738(99)00273-8
69 U. Krašovec, B. Orel, A. Georg, and V. Wittwer: Solar Energy **68** (2000) 541. https://doi.org/10.1016/s0038-092x(00)00033-5
70 S. Lee, H. Cheong, P. Liu, D. Smith, C. Tracy, A. Mascarenhas, J. Pitts, and S. Deb: Electrochim. Acta **46** (2000) 1995. https://doi.org/10.1016/s0013-4686(01)00379-6
71 J. Luo, S. Deng, Y Tao, F. Zhao, L. Zhu, L. Gong, J. Chen, and N. Xu: J. Phys. Chem. C **113** (2009) 15877. https://doi.org/10.1021/jp903581s
72 H. Chen, N. Xu, S. Deng, D. Lu, Z. Li, J. Zhou, and J. Chen: Nanotechnology **18** (2007) 205701. https://doi.org/10.1088/0957-4484/18/20/205701
73 A. Inouye, S. Yamamoto, S. Nagata, M. Yoshikawa, and T. Shikama: Nucl. Instrum. Meth. B **266** (2008) 301. https://doi.org/10.1016/j.nimb.2007.11.016
74 C. Chan, W. Hsu, C. Chang, and C. Hsu: Sens. Actuators, B **157** (2011) 504. https://doi.org/10.1016/j.snb.2011.05.008
75 P. Castillero, V. Rico-Gavira, C. Lopez-Santos, A. Barranco, V. Perez-Dieste, C. Escudero, J. Espinos, and A. Gonzalez-Elipe: J. Phys. Chem. C **121** (2017) 15719. https://doi.org/10.1021/acs.jpcc.7b03385
76 S. Nagata, A. Inouye, S. Yamamoto, B. Tsuchiya, K. Takano, K. Toh, and T. Shikama: J. Alloys Compd. **446**–**447** (2007) 558. https://doi.org/10.1016/j.jallcom.2007.01.039
77 G. Gao, Z. Zhang, G. Wu, and X. Jin: RSC Adv. **4** (2014) 30300. https://doi.org/10.1039/c4ra03181d
78 R. Crandall and B. Faughnan: Phys. Rev. Lett. **39** (1977) 232. https://doi.org/10.1103/PhysRevLett.39.232
79 Y. Xi, Q. Zhang, and H. Cheng: J. Phys. Chem. C. **118** (2013) 494. https://doi.org/10.1021/jp410244c
80 X. Cheng, X. Jiang, K. Tao, Q. Su, Y. Wang, and E. Xie: J. Phys. Chem. Lett. **11** (2020) 9070. https://doi.org/10.1021/acs.jpclett.0c02020
81 S. Deb: Philos. Mag. **27** (1973) 801. https://doi.org/10.1080/14786437308227562
82 H. Wang, G. Gao, G. Wu, H. Zhao, W. Qi, K. Chen, W. Zhang, Y. Li: Int. J. Hydrogen Energy **44** (2019) 15665. https://doi.org/10.1016/j.ijhydene.2019.04.026
83 S. Kalanur, J. Heo, I. Yoo, and H. Seo: Int. J. Hydrogen Energy **42** (2017) 16901. https://doi.org/10.1016/j.ijhydene.2017.05.172

84 S. Kalanur, I. Yoo, Y. Lee, and H. Seo: Sens. Actuators, B **221** (2015) 411. https://doi.org/10.1016/j.snb.2015.06.086
85 C. H. Hsu, C. C. Chang, C. M. Tseng, C. C. Chan, W. H. Chao, Y. R. Wu, M. H. Wen, Y. T. Hsieh, Y. C. Wang, C. L. Chen, M. Wang, and M.-K. Wu: Sens. Actuators, B **186** (2013) 193. https://doi.org/10.1016/j.snb.2013.06.004
86 S. Yamamoto, K. Takano, A. Inouye, and M. Yoshikawa: Nucl. Instrum. Meth. B **262** (2007) 29. https://doi.org/10.1016/j.nimb.2007.04.261
87 D. Li, G. Wu, G. Gao, J. Shen, and F. Huang: ACS Appl. Mater. Interfaces **3** (2011) 4573. https://doi.org/10.1021/am200781e
88 M. Chen, L. Zou, Z. Zhang, J. Shen, D. Li, Q. Zong, G. Gao, G. Wu, and Z. Zhang: Carbon **130** (2018) 281. https://doi.org/10.1016/j.carbon.2018.01.013
89 H. Takahashi, S. Okazaki, Y. Nishijima, and T. Arakawa: Sens. Mater. **29** (2017) 1259. https://doi.org/10.18494/sam.2017.1585
90 A. Wisitsoorat, M. Z. Ahmad, M. H. Yaacob, M. Horpratum, D. Phakaratkul, T. Lomas, A. Tuantranont, and W. Wlodarski: Sens. Actuators, B **182** (2013) 795. https://doi.org/10.1016/j.snb.2013.03.091
91 M. A. Behbahani, M. Ranjbar, P. Kameli, and H. Salamati: Sens. Actuators, B **188** (2013) 127. https://doi.org/10.1016/j.snb.2013.06.097
92 W. Feng, G. Wu, and G. Gao: J. Mater. Chem. A **2** (2014) 585. https://doi.org/10.1039/c3ta13715e
93 L. Nie, X. Guo, C. Gao, X. Wu, J. Chen, and L. Peng: J. Mater. Sci.: Mater. Electron. **33** (2022) 1604. https://doi.org/10.1007/s10854-022-07694-z
94 J. Li, Q. Zhao, G. Zhang, J. Chen, L. Zhong, L. Li, J. Huang, and Z. Ma: Solid State Sci. **12** (2010) 1393. https://doi.org/10.1016/j.solidstatesciences.2010.05.016
95 B. Zhou, W. Feng, G. Gao, G. Wu, Y. Chen, and W. Li: Mater. Res. Express **4** (2017) 115702. https://doi.org/10.1088/2053-1591/aa955c
96 S. Amrehn, X. Wu, and T. Wagner: ACS Sens. **3** (2018) 191. https://doi.org/10.1021/acssensors.7b00845
97 N. T. Garavand, S. M. Mahdavi, A. Iraji zad, and M. Ranjbar: Sens. Actuators, B **169** (2012) 284. https://doi.org/10.1016/j.snb.2012.04.082
98 N. T. Garavand, S. M. Mahdavi, and A. Iraji zad: Appl. Surf. Sci. **273** (2013) 261. https://doi.org/10.1016/j.apsusc.2013.02.027
99 H. Shanak, H. Schmitt, J. Nowoczina, and C. Ziebert: Solid State Ionics **171** (2004) 99. https://doi.org/10.1016/j.ssi.2004.04.001
100 M. Ranjbar, N. T. Garavand, S. M. Mahdavi, and A. Iraji zad: Sol. Energy Mater. Sol. Cells **94** (2010) 201. https://doi.org/10.1016/j.solmat.2009.09.002
101 K. Nishizawa, Y. Yamada, and K. Yoshimura: Sol. Energy Mater. Sol. Cells **170** (2017) 21. https://doi.org/10.1016/j.solmat.2017.05.058
102 K. Nishizawa, Y. Yamada, and K. Yoshimura: Thin Solid Films **709** (2020) 138201. https://doi.org/10.1016/j.tsf.2020.138201
103 J. Y. Luo, L. Gong, H. D. Tan, S. Z. Deng, N. S. Xu, Q. G. Zeng, and Y. Wang: Sens. Actuators, B **171–172** (2012) 1117. https://doi.org/10.1016/j.snb.2012.06.042
104 Ö. Çoban, and S. Tüzemen: Mater. Today: Proc. **46** (2021) 7021. https://doi.org/10.1016/j.matpr.2021.03.283
105 M. Yaacob, M. Ahmad, A. Sadek, J. Ou, J. Campbell, K. Kalantar-zadeh, and W. Wlodarski: Sens. Actuators, B **177** (2013) 981. https://doi.org/10.1016/j.snb.2012.11.098
106 R. Ishihara, Y. Yamaguchi, K. Tanabe, Y. Makino, and K. Nishio: Mater. Chem. Phys. **226** (2019) 226. https://doi.org/10.1016/j.matchemphys.2018.12.052
107 W. Qi, G. Gao, G. Wu, and H. Wang: Sol. Energy Mater. Sol. Cells **195** (2019) 63. https://doi.org/10.1016/j.solmat.2019.01.049
108 Y. Lee, S. Kalanur, G. Shim, J. Park, and H. Seo: Sens. Actuators, B **238** (2017) 111. https://doi.org/10.1016/j.snb.2016.07.058
109 Z. Zhang, D. Guan, G. Gao, G. Wu, and H. Wang: RSC Adv. **7** (2017) 41289. https://doi.org/10.1039/c7ra03648e
110 C. Hu, K. Nishizawa, M. Okada, Y. Yamada, H. Watanabe, K. Tajima, and T. Kawamoto: Inorg. Chim. Acta. **505** (2020) 119466. https://doi.org/10.1016/j.ica.2020.119466
111 G. Gao, S. Xue, H. Wang, Z. Zhang, J. Shen, and G. Wu: J. Sol-Gel Sci. Technol. (2022) https://doi.org/10.1007/s10971-021-05721-9
112 Z. Dehaghi, M. Ranjbar, and M. Goodarzi: Int. J. Hydrogen Energy **46** (2021) 40185. https://doi.org/10.1016/j.ijhydene.2021.09.195
113 X. Sun, L. Hao, L. Chen, X. Guo, C. Han, J. Chen, W. Jiao, R. Wang, and X. He: Appl. Surf. Sci. **599** (2022) 153878. https://doi.org/10.1016/j.apsusc.2022.153878

114 C. Chen, C. Dong, Y. Ho, C. Chang, D. Wei, T.Chan, J. Chen, W. Jang, C. Hsu, K. Kumar, and M. Wu: EPL (Europhysics Letters). **101** (2013) 17006. https://doi.org/10.1209/0295-5075/101/17006

115 W. Jang, Y. Lu, C. Chen, Y. Lu, C. Dong, P. Hsieh, W. Hwang, J. Chen, J. Chen, T. Chan, J. Lee, and W. Chou: Phys. Chem. Chem. Phys. **16** (2014) 4699. https://doi.org/10.1039/c3cp54773f

116 W.-L. Jang, Y.-M. Lu, Y.-R. Lu, C.-L. Chen, C.-L. Dong, W.-C. Chou, J.-L. Chen, T.-S. Chan, J.-F. Lee, C.-W. Pao, and W.-S. Hwang: Thin Solid Films **544** (2013) 448. https://doi.org/10.1016/j.tsf.2013.02.083

117 J. Chen, C. Chang, Y. Ho, C. Chen, C. Hsu, W. Jang, D. Wei, C. Dong, C. Pao, J. Lee, J. Chen, J. Guo, and M. Wu: Phys. Chem. Chem. Phys. **17** (2015) 3482. https://doi.org/10.1039/c4cp04623d

118 Y. Lu, H. Hsu, J. Chen, H. Chang, C. Chen, W. Chou, C. Dong: Phys. Chem. Chem. Phys. **18** (2016) 5203. https://doi.org/10.1039/c5cp06870c

119 A. Sanger, A. Kumar, A. Kumar, J. Jaiswal, and R. Chandra: Sens. Actuators, B **236** (2016) 16. https://doi.org/10.1016/j.snb.2016.05.141

120 P. Ngene, T. Radeva, M. Slaman, R. J. Westerwaal, H. Schreuders, and B. Dam: Adv. Funct. Mater. **24** (2014) 2374. https://doi.org/10.1002/adfm.201303065

121 T. Radeva, P. Ngene, M. Slaman, R. Westerwaal, H. Schreuders, and B. Dam: Sens. Actuators, B **203** (2014) 745. https://doi.org/10.1016/j.snb.2014.06.134

122 C.-W. Hu, Y. Yamada, and K. Yoshimura: J. Mater. Chem. C **4** (2016) 5390. https://doi.org/10.1039/c6tc01541g

123 C.-W. Hu, Y. Yamada, and K. Yoshimura: Sol. Energy Mater. Sol. Cells **177** (2018) 120. https://doi.org/10.1016/j.solmat.2017.01.021

124 S. Yang, G. Chen, F. Zheng, Y. Yu, S. Ye, T. Wang, Y. Fu, and X. Zhang: Sens. Actuators, B **368** (2022) 132242. https://doi.org/10.1016/j.snb.2022.132242

125 Z. Gao, T. Wang, X. Li, Q. Li, X. Zhang, T. Cao, Y. Li, L. Zhang, L. Guo, and Y. Fu: ACS Appl. Mater. Interfaces **12** (2020) 42971. https://doi.org/10.1021/acsami.0c13137

126 J. Reichstein, S. Schötz, M. Macht, S. Maisel, N. Stockinger, C. C. Collados, K. Schubert, D. Blaumeiser, S. Wintzheimer, A. Görling, M. Thommes, D. Zahn, J. Libuda, T. Bauer, and K. Mandel: Adv. Funct. Mater. **32** (2022) 2112379. https://doi.org/10.1002/adfm.202112379

127 C.-W. Hu, Y. Yamada, and K. Yoshimura: Sol. Energy Mater. Sol. Cells **187** (2018) 30. https://doi.org/10.1016/j.solmat.2018.07.022

128 C.-W. Hu, Y. Yamada, and K. Yoshimura: Chem. Commun. **53** (2017) 3242. https://doi.org/10.1039/c7cc00077d

129 C.-W. Hu, K. Yoshimura, A. Takahashi, H. Watanabe, K. Tajima, and T. Kawamoto: J. Mater. Chem. C. **6** (2018) 4760. https://doi.org/10.1039/c8tc00648b

130 M. Ranjbar, S. M. Mahdavi, and A. Iraji zad: Sol. Energy Mater. Sol. Cells **92** (2008) 878. https://doi.org/10.1016/j.solmat.2008.02.018

131 S. G. Zamharir, M. Ranjbar, and H. Salamati: Sol. Energy Mater. Sol. Cells **130** (2014) 27. https://doi.org/10.1016/j.solmat.2014.06.029